Disaggregated Seismic Hazard and the Elastic Input Energy Spectrum: An Approach to Design Earthquake Selection

Martin C. Chapman

Thesis submitted to the Faculty of the Virginia Polytechnic Institute and State University in partial fulfillment of the requirements for the degree of

Doctor of Philosophy
in
Geophysics

J. Arthur Snoke, Chair
Gilbert A. Bollinger
Edwin S. Robinson
James R. Martin
Mahendra P. Singh

June 25, 1998
Blacksburg, Virginia

Keywords: Seismic Hazard, Strong Motion, Design Earthquakes, Input Energy

Disaggregated Seismic Hazard and the Elastic Input Energy Spectrum: An Approach to Design Earthquake Selection

Martin C. Chapman

(Abstract)

The design earthquake selection problem is fundamentally probabilistic. Disaggregation of a probabilistic model of the seismic hazard offers a rational and objective approach that can identify the most likely earthquake scenario(s) contributing to hazard. An ensemble of time series can be selected on the basis of the modal earthquakes derived from the disaggregation. This gives a useful time-domain realization of the seismic hazard, to the extent that a single motion parameter captures the important time-domain characteristics. A possible limitation to this approach arises because most currently available motion prediction models for peak ground motion or oscillator response are essentially independent of duration, and modal events derived using the peak motions for the analysis may not represent the optimal characterization of the hazard.

The elastic input energy spectrum is an alternative to the elastic response spectrum for these types of analyses. The input energy combines the elements of amplitude and duration into a single parameter description of the ground motion that can be readily incorporated into standard probabilistic seismic hazard analysis methodology. This use of the elastic input energy spectrum is examined. Regression analysis is performed using strong motion data from Western North America and consistent data processing procedures for both the absolute input energy equivalent velocity, (V_{ea}), and the elastic pseudo-relative velocity response (PSV) in the frequency range 0.5 to 10 Hz. The results show that the two parameters can be successfully fit with identical functional forms. The dependence of V_{ea} and PSV upon (NEHRP) site classification is virtually identical. The variance of V_{ea} is uniformly less than that of PSV, indicating that V_{ea} can be predicted with slightly less uncertainty as a function of magnitude, distance and site classification. The effects of site class are important at frequencies less than a few Hertz. The regression modeling does not resolve significant effects due to site class at frequencies greater than approximately 5 Hz.

Disaggregation of general seismic hazard models using V_{ea} indicates that the modal magnitudes for the higher frequency oscillators tend to be larger, and vary less with oscillator frequency, than those derived using PSV. Insofar as the elastic input energy may be a better parameter for quantifying the damage potential of ground motion, its use in probabilistic seismic hazard analysis could provide an improved means for selecting earthquake scenarios and establishing design earthquakes for many types of engineering analyses.

Acknowledgments

I thank my graduate studies committee Drs. J. Arthur Snoke, Edwin S. Robinson, James R. Martin, Mahendra P. Singh, and most of all, Dr. Gilbert A. Bollinger, for his long-term support and guidance. Funding for these studies was provided by the Federal Emergency Management Agency, the Virginia Department of Emergency Services, and the U. S. Geological Survey. The Generic Mapping Tools software (Wessel and Smith, 1991) was used to prepare many of the figures.

Table of Contents

List of Figures

List of Tables

Chapter 1: Introduction

The solution of many earthquake engineering problems involves dynamic analysis and testing using ground motion time series. The time series, or design earthquake, should be selected to reflect the characteristics of potential ground motions at a specific site. Important characteristics include amplitude of motion, frequency content and duration of shaking. The characteristics are determined by the earthquake source process, the wave propagation effects of the path between the source and the site and the site response.

The design earthquake selection process involves consideration of the seismic hazard in the site area and the general response characteristics of the structure(s) being analyzed. In most situations the seismic hazard is uncertain, and is posed by the possible occurrence of earthquakes at more than one location; likewise, the sizes, or magnitudes, of potentially damaging shocks may be widely distributed. Distance and magnitude have a very important impact upon the nature of strong motion at a specific site. Selecting time series for design is essentially a problem of choosing appropriately from among a number of future earthquake scenarios. The most important elements of the scenario are the magnitude of the earthquake and the distance from the source of energy release to the site. Both of these elements are random variables: therefore, design earthquake scenarios are best developed from a formal probabilistic model of the seismic hazard.

The research presented here addresses issues involved in the design earthquake selection process. In Chapter 2, a probabilistic approach is presented that can provide an objective basis for that selection. It offers the advantage that uncertainties can be accounted for quantitatively, and the distinctions between competing interpretations of the seismic hazard can be readily examined. The design earthquake scenarios are then derived using the concept of the modal event, which represents the most likely combination of earthquake magnitude and source-site distance contributing to the total hazard. To reflect the seismic hazard posed to complex structures, these modal event scenarios are generated for a range of oscillator frequencies and damping values.

It is widely recognized that duration plays an important role in the damage potential of ground motion for some types of construction. However, duration is not routinely modeled in conventional probabilistic hazard analyses. In Chapter 3 of this study, the duration of shaking is involved directly in the design earthquake selection through the use of a motion prediction model based on elastic input energy. Empirical prediction models for pseudo-velocity and a parameter

based on elastic input energy are developed using the strong motion data set of western North America and compared using consistent processing approaches. The prediction models are developed for oscillator frequencies in the range 0.5 to 10 Hz, and for 3 values of damping. The impact of the duration dependent parameter on the probabilistically developed scenario events is assessed.

Chapter 4 concludes the study and presents a summary of results.

Chapter 2: Design Event Selection

2.1 Background

Probabilistic seismic hazard analysis (PSHA) has in recent years become the primary method by which earthquake hazard is quantified. It is also the means by which hazard information is communicated, among the seismological and earthquake engineering communities and the general public. Traditionally, the end result of a PSHA was a curve depicting the probability of exceeding some range of motion parameter values, from all possible earthquakes at all possible locations. Because of the integrative nature of the analysis results, contributions to seismic hazard from specific magnitude earthquakes at specific distances are obscure. However, for many engineering problems, it is necessary to select one or more scenario earthquakes as a basis for synthesizing or selecting ground motion time series.

Recently, much interest has focused on the use of the "disaggregated" PSHA as a tool for selecting earthquake scenarios for design purposes. The process of disaggregaton is undertaken to identify important elements of the seismic hazard model contributing to total hazard for a given probability of exceedance. The National Research Council (1988) recommended that the dominant contributing earthquake (in terms of magnitude and distance) be determined in PSHA, as a means to gain further insight into the nature of the seismic hazard. At that time, a considered candidate for the dominant earthquake was the mean magnitude and distance of the seismic events causing ground motion exceedance at a specified return period, a concept introduced earlier by McGuire and Shedlock (1981).

An example of a somewhat different conceptual representation of the dominant hazard was the work of Milne and Wiechert (1986). They determined the relative contribution to total exceedance probability in the joint magnitude-distance domain for several sites included in the National Building Code of Canada seismic probability map.

Recently, Stepp et al. (1993) and Chapman (1995) discussed disaggregation approaches with the objective of addressing issues involved in the design earthquake selection process. Those studies disaggregated the hazard into magnitude and distance space for independent oscillator frequencies, and in the study by Stepp et al., the disaggregation was extended to include the random variable ε, representing the variability of ground motion prediction models. Chapman

(1995) advocated the use of the modal event, the most likely combination of earthquake magnitude and source-site distance contributing to hazard at a given return period, as a basis for design event selection. In that approach, an ensemble of design events would be derived for different frequencies of the elastic response spectrum, thereby giving a relatively complete description of the seismic hazard, under the assumption that exceedances of response spectral ordinates at different frequencies are statistically independent. Chapman (1995) included ε as a random variable, but used the modes of the marginal magnitude-distance hazard density function to define the ensemble design events. McGuire (1995) advocated the use of the joint magnitude-distance-ε density function for this purpose, and presented a method whereby a single design earthquake closely matching the uniform hazard response spectrum could (under some circumstances) be defined on the basis of a modal event in magnitude-distance-ε space. His approach involved hazard calculation based on joint exceedance at two distinct oscillator frequencies.

The presentation of hazard estimates in terms of the disaggregated PSHA is becoming a standard practice. The National Seismic Hazard Mapping Project of the U.S. Geological Survey (Frankel et al., 1996) has made available disaggregated seismic hazard results for major cites nationwide on the World-Wide-Web at *http://geohazards.cr.usgs.gov*. Disaggregated seismic hazard results in the form of maps showing dominant source distance and magnitude for southern California were prepared by Cramer and Petersen (1996). A recent study by Bazzurro and Cornell (1998) examines the various proposed disaggregation approaches. They point out that significantly different results can be obtained, depending upon details of the method used, and advocate a disaggregation in terms of latitude, longitude, magnitude and ε, to permit identification of hazard-dominating scenario events and to associate them with one or more specific faults, rather than a given distance.

The fundamental elements of PSHA are reviewed in the following section of this Chapter. Then, the concept of a modal event derived from the hazard density function is introduced, and an example of design event selection using that concept is presented. Chapter 3 of this study develops duration dependent ground-motion prediction models and assesses their impact upon the definition of the modal event, using generalized disaggregated PSHA models.

2.2 Fundamentals of Probabilistic Hazard Analysis

The method of quantifying seismic hazard has undergone much development and application since being introduced by Cornell (1968). The objective of the probabilistic seismic hazard analysis (PSHA) is to estimate the probability of exceeding a specified motion intensity, by taking into account the potential occurrence of earthquakes at all possible locations, having all possible magnitudes. Earthquake magnitude, source-site distance and motion intensity are the major random variables in the PSHA.

A basic method common to most analyses is described below. A complete treatment of statistical variability and uncertainty on all model parameters can be incorporated using Bayesian estimation methods and Monte Carlo simulation (e.g., Coppersmith and Youngs, 1986; Bernreuter et al., 1989; National Research Council, 1988). In the more sophisticated analyses, the basic method may be performed several hundred to several thousand times, each time sampling the model parameters from their distributions. In this way, the effects of random variability and model uncertainty are quantified, in terms of a distribution function for exceedance probabilities.

In a conventional PSHA, exceedances of a specified motion intensity are assumed to follow the Poisson stochastic process. The Poisson process is characterized by the following behavior: 1) an event can occur at any time; 2) the occurrence of an event is independent of any other event, and 3) the probability of an event occurring in a small time interval Δt, is given by $\nu\Delta t$, where ν is the (constant) mean rate of occurrence. The Poisson process is defined by the Poisson probability distribution:

$$P(X_t = x) = \frac{(\upsilon t)^x}{x!} e^{-\upsilon t} \qquad \text{for } x=0,1,2..... \qquad (2.1)$$

where ($P(X_t = x)$ is the probability of integer "x" events in time "t". For x=0, $P(X_t = 0) = e^{-\nu t}$. The probability of at least one event in time "t" is therefore given by

$$P(X_t \neq 0) = 1 - e^{-\upsilon t} \quad . \qquad (2.2)$$

In a conventional PSHA, the task is to estimate ν_g, the mean rate of exceeding some motion intensity g at a specific site. A general expression for ν_g is (Rieter, 1990; Chapman, 1995; McGuire, 1995),

$$\upsilon_g = \sum_{i=1}^{N} \alpha_i \left\{ \int_{m^-}^{m^+} \int_{r^-}^{r^+} \int f_{M,R,\varepsilon}(m,r,\varepsilon)\, H(G>g|m,r,\varepsilon)\, dm\, dr\, d\varepsilon \right\}_i . \qquad (2.3)$$

In Equation 2.3, it is assumed that seismic hazard is contributed by N independent sources of earthquakes. The mean rate of earthquakes in each source is α_i and $f_{M,R,\varepsilon}$ is the joint probability density of earthquake magnitude M, source to site distance R and random error ε associated with motion prediction. Motions are predicted using a relation of the form

$$\text{Log } G = Y(m,r) + \varepsilon\sigma, \qquad (2.4)$$

typically derived by regression analysis of strong motion data (e.g., Abrahamson and Shedlock, 1997). In addition to magnitude and distance, a motion prediction model may also include other variables such as site condition and fault type. The random error of the prediction model is represented by a standardized normal variate ε with standard deviation σ. In Equation 2.3, the function $H(G>g|m,r,\varepsilon)$ is unity if $Y(m,r) + \varepsilon\sigma$ is greater than Log g, and is zero otherwise.

The basic model represented by Equation 2.3 is flexible and can be adapted to a variety of practical situations incorporating any number of different tectonic interpretations. In general, the joint density function $f_{M,R,\varepsilon}$ is complicated and must be evaluated numerically.

For the purposes of this study, ε will be assumed independent of magnitude and distance. This assumption is consistent with most currently available strong motion prediction models (Abrahamson and Shedlock, 1997). In many cases, it is practical to treat distance and magnitude as statistically independent as well. This simplified approach is warranted in cases where the geologic sources potentially responsible for damaging shocks are obscure or poorly understood. In such cases, discrete fault models cannot be developed, and an alternative is to treat seismicity as spatially uniform on a local scale. Area sources are defined wherein the earthquakes occur spatially with uniform probability: the rates α_i of earthquakes within the area sources are defined on the basis of the earthquake history.

An alternative to area sources is known as "spatial smoothing." In that approach the treatment of distance r as a random variable is handled by replacing the α_i in Equation 2.3 by a seismicity rate density that is a continuous function of latitude and longitude. The total exceedance rate ν_g is determined by numerical integration over magnitude, latitude, longitude and ε (Frankel et al., 1996; Woo, 1996).

In situations where geologic evidence and/or the earthquake history warrants such treatment, fault sources can be modeled (e.g., Bender, 1984). In more physically realistic models, fault rupture length is dependent upon earthquake magnitude: as a result, source to site distance r depends upon magnitude m.

For clarity in the present discussion, as well as in some examples that follow in later sections, magnitude, distance and ε will be treated as statistically independent. It is important to recognize that this assumption is not necessary, and does not limit the results and procedures of this study. Also, for examples shown in this study, the hazard will be posed by discrete sources. A formulation in terms of the spatial smoothing approach is straightforward. The issue of dependent model parameters will be addressed in later sections, in the context of model disaggregation and relevance to design earthquake selection.

Treating distance, magnitude and ε as statistically independent, the estimated rate of exceeding motion intensity g due to hazard posed by N independent, discrete sources is

$$\upsilon_g = \sum_{i=1}^{N} \alpha_i \left\{ \int_{m^-}^{m^+} \int_{r^-}^{r^+} \int f_M(m) f_R(r) f_\varepsilon(\varepsilon) H(G>g|m,r,\varepsilon)\, dm\, dr\, d\varepsilon \right\}_i . \qquad (2.5)$$

The source-site distance probability density f_R is defined by the spatial geometry of the source, with respect to the site location. In this standard formulation, it is non-zero between limits of integration r^- and r^+, representing the nearest and furthest approaches of an earthquake source to the site.

The magnitude density f_M depends upon the earthquake recurrence model. Often, f_M is assumed to be exponential, truncated at lower and upper limits of integration m^- and m^+: however, that functional form is not a required assumption. The truncated exponential form of f_M follows from the empirical Gutenberg-Richter earthquake recurrence relationship, Log n = a-bm, relating n, the rate of earthquakes with magnitudes exceeding m, to magnitude (Gutenberg and Richter, 1954). The upper magnitude truncation of the distribution reflects the constraint of finite release of seismic energy. Another magnitude density function of interest is that related to the characteristic earthquake model (Youngs and Coppersmith, 1985) which is used to model hazard from well-documented active fault segments (e.g., Working Group for California Earthquake Probabilities,

1996; Frankel et al., 1996). The lower limit of magnitude integration, m^-, is usually taken to be approximately 4.5, representing the smallest earthquakes typically considered to be of engineering concern. However, some care must be taken in specifying m^-. As shown by Chapman (1995) m^- and g must be specified jointly such that $Y(m^-,r^-) < \text{Log } g$. Failure to satisfy this condition may lead to significant underestimation of hazard. The upper magnitude truncation, m^+, is a very important parameter. Ideally, it is estimated using relevant geologic and paleoseismologic data, geodetic strain rates and the seismic history of the region (Yeats et al., 1997; Working Group on California Earthquake Probabilities, 1995). However, in most cases it is uncertain and may be treated as a random variable in the hazard analysis (e.g., Bernreuter et al., 1989). For the truncated exponential density function, f_M is given by

$$f_M(m) = \frac{b' e^{-b'm}}{e^{-b'm^-} - e^{-b'm^+}}, \quad m^- < m < m^+, \tag{2.6}$$

where $b' = \ln(10)b$. From Equations 2.3 and 2.5 it is clear that ν_g is proportional to the seismicity rate α. The truncated exponential magnitude density, reflecting a constrained Gutenberg-Richter earthquake recurrence model, implies

$$\alpha = 10^{a-bm^-} - 10^{a-bm^+}. \tag{2.7}$$

Finally, it is assumed here that f_ε is the standard normal probability density function. It is sometimes desirable to modify this distribution by truncating the tails and normalizing. This is done to include the well-documented log-normal behavior of strong motion peak response values, but limit the hazard model to motions that have been observed or that can reasonably be considered possible on the basis of the empirical dataset. Typically, the density distribution is truncated at approximately mean $\pm 2\sigma$. That sort of model would imply lower and upper integration limits for ε of -2 and +2 in Equations 2.3 and 2.5, and the necessary normalization of f_ε. In the examples that follow, the untruncated standard normal distribution is used.

2.3 PSHA Disaggregation and the Modal Event

The identification of the events, in terms of magnitude and distance, that contribute most to seismic hazard for a given probability of exceedance has practical application. It can serve as a guide for defining scenarios and design earthquakes for engineering problems, particularly those involving dynamic analysis using ground motion time series. For example, a user may wish to

select an actual strong-motion time series, that is in some sense "compatible" with a specific probability of exceedance. This is a problem that in general has no unique deterministic solution. As indicated by Equation 2.3, seismic hazard is the result of potential earthquakes that may exhibit a range of magnitudes and may occur over a range of distances from a site. Clearly, the problem of selecting one or more specific earthquake events, as required for some engineering applications, is fundamentally probabilistic in nature. Therefore, a probabilistic approach to the decision process is required.

As shown below, it is possible to identify the most likely (i.e., most frequent) events, defined in terms of magnitude and distance, that contribute to seismic hazard. The information can be obtained by "disaggregating" the results of a seismic hazard calculation. In the following, PSHA disaggregation and modal event identification is discussed, and demonstrated using a simple hypothetical example.

For simplicity, assume a hazard model wherein the random variables are statistically independent and limited to those appearing in the motion prediction model (m, r and ε, Equation 2.4). For those conditions, Equation 2.5 completely defines the expected rate of exceeding a specific motion intensity g.

Let U(m,r,ε | g) represent the integrand of Equation 2.5, for a specific value of g. This value g could correspond to some chosen probability of exceedance: e.g., P(G>g)=0.001 (1000 year return period). Thus,

$$U(m,r,\varepsilon \mid g) = \sum_{i=1}^{N} \alpha_i \left\{ f_M(m) f_R(r) f_\varepsilon(\varepsilon) H(G>g|m,r,\varepsilon) \right\}_i . \qquad (2.8)$$

Equation 2.8 represents the joint "hazard density" or "disaggregated hazard" for a specified motion intensity g. In analogy to the definition of the mode of a random variable, let ($\underline{m},\underline{r},\underline{\varepsilon}$) define the location of the maximum value of U(m,r,ε | g). This is the "modal event" (or β-point; McGuire, 1995) locating the mode of the joint hazard distribution for the exceedance of selected motion value g. Integration with respect to the random variables yields the expected value of the exceedance rate.

A marginal distribution U'(m,r | g) can be obtained by integration of Equation 2.8 with respect to standardized random variable ε, or

$$U'(m,r \mid g) = \int U(m,r,\varepsilon \mid g)\, d\varepsilon = \sum_{i=1}^{N} \alpha_i \left\{ f_M(m)\, f_R(r) \int f_\varepsilon(\varepsilon)\, H(G>g|m,r,\varepsilon)\, d\varepsilon \right\}_i$$

$$= \sum_{i=1}^{N} \alpha_i \left\{ f_M(m)\, f_R(r) \left[1 - \Phi\left(\frac{\text{Log } g - Y(m,r)}{\sigma}\right)\right] \right\}_i . \qquad (2.9)$$

In Equation 2.9, Φ is the cumulative normal probability distribution function. Let the maximum value of U'(m,r | g) occur at ($\underline{m}'$,$\underline{r}'$). In general, $\underline{m}'$ and $\underline{r}'$ are not equivalent to $\underline{m}$ and $\underline{r}$. This is an important point. The magnitudes and distances of the modal events derived in the disaggregation using marginal distributions may differ from those of the joint distribution. Most recent work suggests that the appropriate disaggregation approach for design event selection is that based on the joint hazard density function U(m,r,ε | g). Chapman (1995) advocated the use of the marginal distribution U'(m,r | g) for this purpose because the physical significance of ε is that of a scaling parameter that captures the effects of unmodeled physical processes. In actual practice, use of U' to determine the modal magnitude $\underline{m}'$ and distance $\underline{r}'$ has an advantage in regard to the scaling necessary to create a time series compatible with the specified motion g. On the other hand, the modal magnitude $\underline{m}$ and distance $\underline{r}$ derived from U represents a "more likely" earthquake (in terms of probability of occurring). This issue will be explored using an example calculation.

A hypothetical example is suggested by Figure 2.1, adapted from Chapman, (1995). One approach could be to model the hazard using two independent sources: a line source with nearest approach to the site of 30 km, and a "background" source area, enclosed by a circle of radius 200 km centered on the site. The example represents an active fault, embedded in a relatively less seismic region. For both sources, we will assume the following recurrence relationship:

$$\text{Log } n = 4.101 - 0.8\, m, \qquad (2.10)$$

where n is events per year, implying two magnitude 6 or greater earthquakes per decade within each source. We will assume a truncated exponential density function for magnitude of the form of Equation 2.6, where b' = 0.8 ln(10). For the line source, let $m^- = 5.0$ and $m^+ = 7.7$. In the background, let $m^- = 5.0$ and $m^+ = 6.5$. The expected rate α of earthquakes with magnitudes between m^- and m^+ is given by Equation 2.7.

The probability density of epicentral distance for the background source is

$$f_R(r) = \frac{2r}{r_{max}^2}, \qquad 0 \le r \le r_{max}, \tag{2.11}$$

where r_{max} is the radius of the source area (200 km). For the line source, assuming that earthquakes can occur anywhere along the line with uniform probability, independent of magnitude, we have:

$$f_R(r) = \frac{2r}{L\sqrt{r^2-30^2}}, \quad 30 \le r \le \sqrt{30^2+L^2/4}, \tag{2.12}$$

where L is the length of the line (387 km).

Finally, assume that the motion parameter G is a log-normally distributed random variable. Let G be pseudo-relative velocity response. The mean logarithm of G is derived from the prediction equations of Joyner and Boore (1982) for 5% damping and rock site conditions.

Figure 2.2 shows the hazard curves for the above example, computed for 1, 5, and 10 Hz oscillators. The marginal hazard density functions U'(m,r | g) for the three oscillator frequencies are shown in Figure 2.3, where g is PSV response such that P(G>g) = 0.002 for a 500 year return period. The total volume represented in each plot is equal to 0.002. The three hazard density functions are bi-modal, clearly reflecting the contributions to hazard from the two sources.

The line source (fault) dominates the hazard for the 1 Hz oscillator. The modal events for the 1 Hz oscillator (due to the line source) are $\underline{m}'$=6.86, $\underline{r}'$=30, for the maximum of U', and $\underline{m}$=6.75, $\underline{r}$=30, $\underline{\varepsilon}$=1.32, based on disaggregation using the joint density function U. The corresponding value of PSV for the 500 year return period is 32.5 cm/sec (Figure 2.2). Utilizing this information to select a time series consistent with a return period of 500 years involves accounting for the effects of the random error variable ε. We next consider the procedure advocated by Chapman (1995) using the marginal density function U'.

Let g'_{mode} represent the median oscillator response for the modal event defined by ($\underline{m}'$,$\underline{r}'$) for the 1 Hz oscillator. The motion prediction model predicts a median value of 13.2 cm/sec for 1 Hz PSV response, given the occurrence of the modal event. This is slightly less than half the response amplitude for the chosen exceedance frequency (g=32.5 cm/sec). In the example, this difference between the median motion prediction for the modal event, g'_{mode}, and g arises because the predicted oscillator response is treated as a random variable: i.e., the ground motion prediction

model includes the random variable ε. This element of the seismic hazard model complicates the problem of design event selection, but is necessary because motion intensity at a given distance from an earthquake exhibits statistical variation or "scatter", here represented by ε. Although the scatter associated with a particular motion prediction model can, in principle, be reduced by modeling additional information on the earthquake source, propagation path and site response, it cannot be eliminated entirely. A significant reduction in the scatter is particularly difficult when the locations and magnitudes (and associated source and path effects) of future earthquakes are uncertain.

In the example, the base 10 logarithm of oscillator response is assumed to be normally distributed with $\sigma = 0.33$. The logarithm of oscillator response corresponding to $P(G>g) = 0.002$ is approximately 1.18 standard deviations above the predicted mean logarithm of response for the modal event ($\underline{m}'$,$\underline{r}'$). Therefore, given the occurrence of the modal event, there is approximately a 12% probability that the resulting PSV response at the site will exceed g = 32.5 cm/sec, for $P(G>g) = 0.002$. For dynamic analyses at frequencies near 1 Hz, a ground motion time series consistent with the results of the example hazard analysis could be selected at the 88% percentile from the population of time series recorded at $\underline{r}'$=30 km from magnitude $\underline{m}'$=6.86 earthquakes. Because this population is small, a more practical approach is to select or synthesize a "best estimate" ground motion time series representative of the modal event, and scale the amplitude of the time series such that the PSV response is g=32.5 cm/sec corresponding to the design P(G>g).

It is important to note that this approach is strictly valid only for a narrow frequency band. Further, as shown by Chapman (1995), the interpretation of the difference between g'_{mode} and g as due entirely to the modeling of random scatter in the motion prediction model holds only for hazard models wherein three conditions are satisfied. First, the partial derivative with respect to magnitude of the joint hazard density function U'(m,r) of *each* source contributing to hazard at a given site must be negative: i.e., $f_M(m)f_R(r)$ or $f_{R,M}(m,r)$ for each source must decrease with increasing magnitude. This condition is always satisfied for the common situation where distance and magnitude can be treated as statistically independent and the magnitude density functions of the various sources are assumed exponential. However, a subset of the group of models wherein distance and magnitude are statistically dependent may not satisfy this condition in all cases. The second condition, implied by Equation 2.9, is that $f_\varepsilon(\varepsilon)H(G>g|m,r,\varepsilon)$ remain invariant among the sources contributing to hazard. This amounts to using the same attenuation model Y(m,r) and ε distribution function to predict ground motion for each source. Finally, the third condition is that

$Y(\bar{m},\bar{r}) < \text{Log } g$. All three of these conditions are satisfied by a broad range of useful seismic hazard models, in addition to the simple example given above. In cases not satisfying these conditions, scaling of time series remains a viable, but ad hoc, approach, and it should be recognized that the difference between g'_{mode} and g in those cases may not be entirely due to the modeling of random error via the inclusion of the variable ε.

Stepp et al., (1993), McGuire (1995) and Bazzurro and Cornell (1998) advocate disaggregation using $U(m,r,\varepsilon \mid g)$. In practice, the event $(\underline{m},\underline{r})$ derived from the joint hazard density $U(m,r,\varepsilon \mid g)$ is more likely to occur than the marginal event represented by $(\underline{m}',\underline{r}')$. In the example above, for 1 Hz, $\underline{r}$ and $\underline{r}'$ are equal (30 km) and $\underline{m}$=6.75, whereas $\underline{m}'$=6.86. Note that $(\underline{m}',\underline{r}')$ defines a larger, less frequent earthquake. Another advantage of the 3-dimensional disaggregation is that it eliminates the ad hoc scaling involved in the use of $U'(m,r \mid g)$. The scaling factor is rigorously defined by use of the jointly determined estimate $\underline{\varepsilon}\sigma$. However, in most hazard models, particularly those satisfying the three conditions mentioned above, the scaling factor $10^{\sigma\underline{\varepsilon}}$ is larger than the ad hoc value derived on the basis of the modal event $(\underline{m}',\underline{r}')$ from the marginal density function U'. Use of $(\underline{m},\underline{r})$ as a basis for design event time series selection will usually involve a larger scaling of a chosen "best estimate" time series.

In the 1 Hz example above, $\underline{\varepsilon}$ is 1.32 and σ is 0.33. This represents a factor of $10^{1.32x0.33}$ = 2.73, for multiplying the median motion estimate $10^{Y(\underline{m},\underline{r})}$. The ad hoc scaling factor that equates g'_{mode} = 13.2 cm/sec and g=32.5 cm/sec is 2.46. In the context of time series selection, the joint 3-dimensional modal event $(\underline{m},\underline{r},\underline{\varepsilon})$ offers the advantage of identifying the "most likely" or dominate event, but in many situations requires a larger scaling of a median or "best estimate" time series to achieve a time domain realization of the hazard. Also, in models where the basis variable G is a peak motion value, the random variable ε is not clearly correlated with other characteristics of the strong motion time series (such as duration), as are the remaining variables (magnitude, distance). Hence, it can be argued that under these conditions, the use of U', while ad hoc, may provide a physically more realistic time domain realization of the hazard. A practical limitation exists regardless of the issue of applying U or U' to this problem, because other variables are needed in the hazard model to better define the characteristics of the strong motion in the time domain. This important issue will be addressed in Chapter 3.

The general disaggregation approach described above can provide information on the most likely ground motions at a given site corresponding to a pre-defined hazard level and oscillator

frequency. However, complex structures may exhibit several response modes. This, combined with the fact that both the shape and amplitude of the ground motion spectrum change as functions of distance and magnitude means that several time series may be necessary to represent properly, for engineering purposes, the most likely motions indicated by the hazard analysis.

The shape of the ground motion spectrum and therefore, the response spectrum, is strongly dependent upon distance and magnitude. The maxima of $U(m,r,\varepsilon \mid g)$ and $U'(m,r \mid g)$ will vary depending upon the frequency of the oscillator, as well as upon the response amplitude g. This means that for a fixed probability of exceedance, the modal event for a high frequency oscillator will generally differ from that of a low frequency oscillator. The same can be said for any motion parameter that is frequency dependent. Typically, the modal events for the higher frequencies will tend to be of smaller magnitude at smaller distances, compared to the modal events for the lower frequency motion parameters. Generally, a unique modal event cannot be defined for the entire response spectrum at a fixed exceedance frequency: i.e., a single modal event will not generally match the uniform hazard response spectrum. For this reason, multiple design time series should be developed for the specific frequency band(s) of engineering concern in regard to structural response.

These points are illustrated in Figure 2.3, which shows that the contribution to seismic hazard shifts to smaller earthquakes, at smaller distances, as oscillator frequency increases. This is a consequence of attenuation of the higher frequency ground motion, and the shape and magnitude scaling of the earthquake source spectrum. In the example, there is clearly a need to consider two design events for the 10 Hz oscillator: a magnitude 6.2 shock at 30 km, due to the line source, and a magnitude 5.4 event at 8 km in the background. The events have comparable contributions to seismic hazard at 10 Hz, yet their time series can be expected to be very different: e.g., the larger, more distant shock would generate strong motions of much longer duration. Thus, the two events could have very different consequences for certain types of construction.

In some cases, particularly those in which non-linear behavior of structures or soils must be considered, the duration of shaking as well as the amplitude of motion can be an important consideration for design. The approach described in the example above does not take duration into account because the random variables serving as the basis for the hazard estimates (peak oscillator response) are essentially independent of the duration of ground shaking. As described in the following Chapter, a duration dependent parameter such as a measure of input energy might be a

more useful basis variable for the hazard analysis. An approach similar to that discussed previously could be performed to identify the modal events and select appropriate time series, provided that the duration dependent parameter is predictable as a function of magnitude and distance.

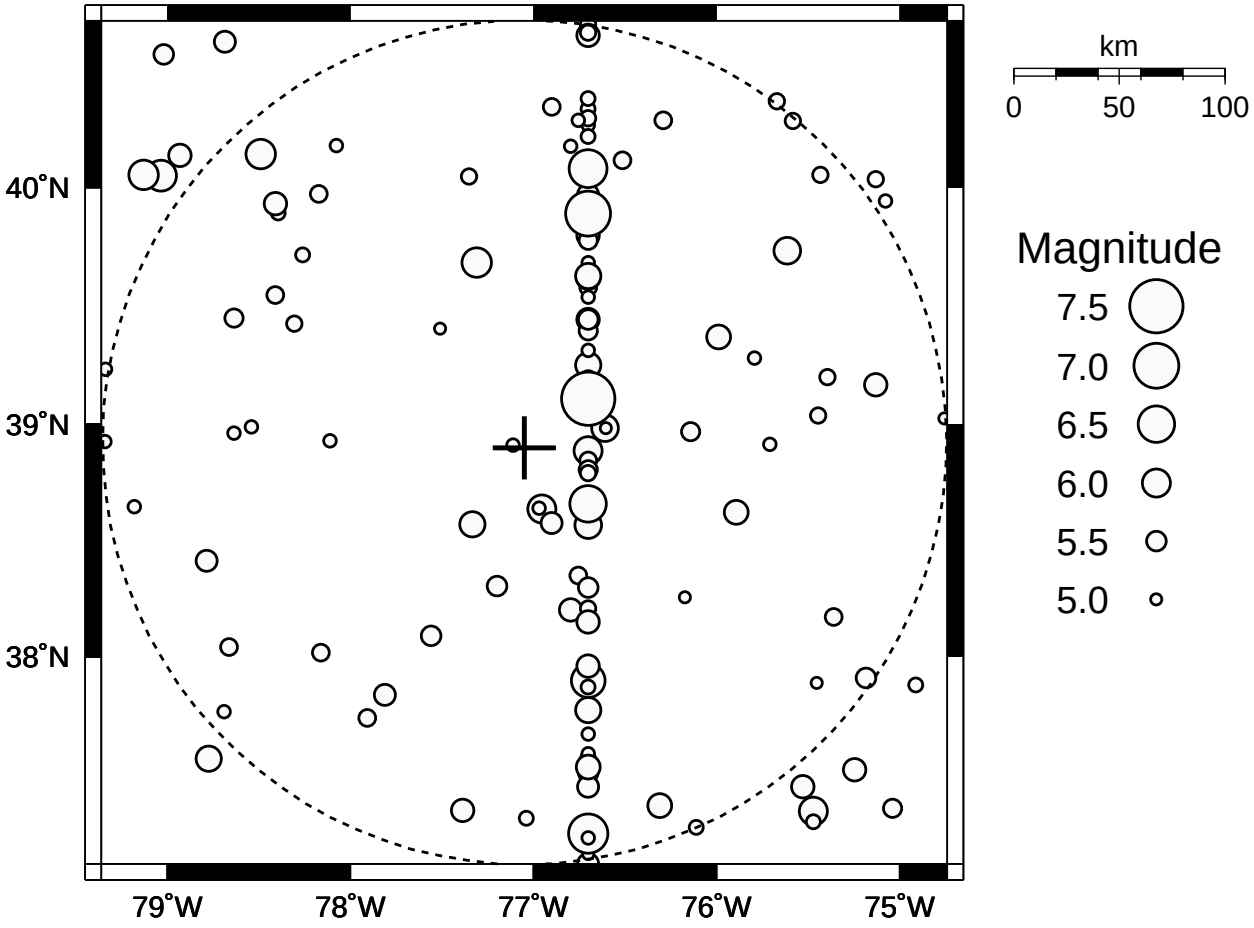

Figure 2.1: Hypothetical 50 year seismicity map consistent with the two-source example seismic hazard calculation. The "site" is indicated by the cross. The dashed line indicates the "background" source: the linear trend of epicenters is modeled as a line source. Modified from Chapman (1995).

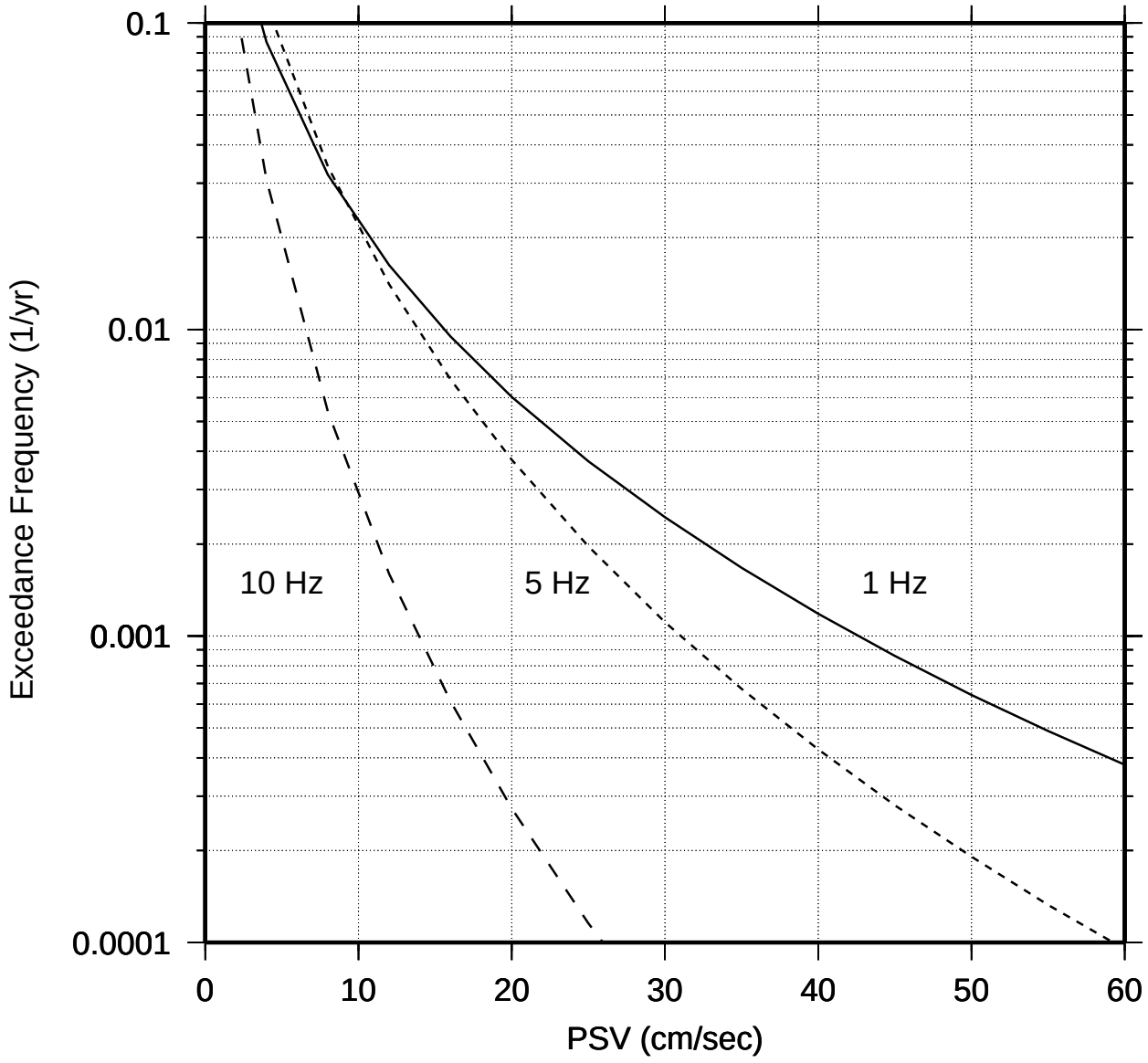

Figure 2.2: Seismic hazard curves, (PSV response) for the example discussed in the text. Modified from Chapman (1995).

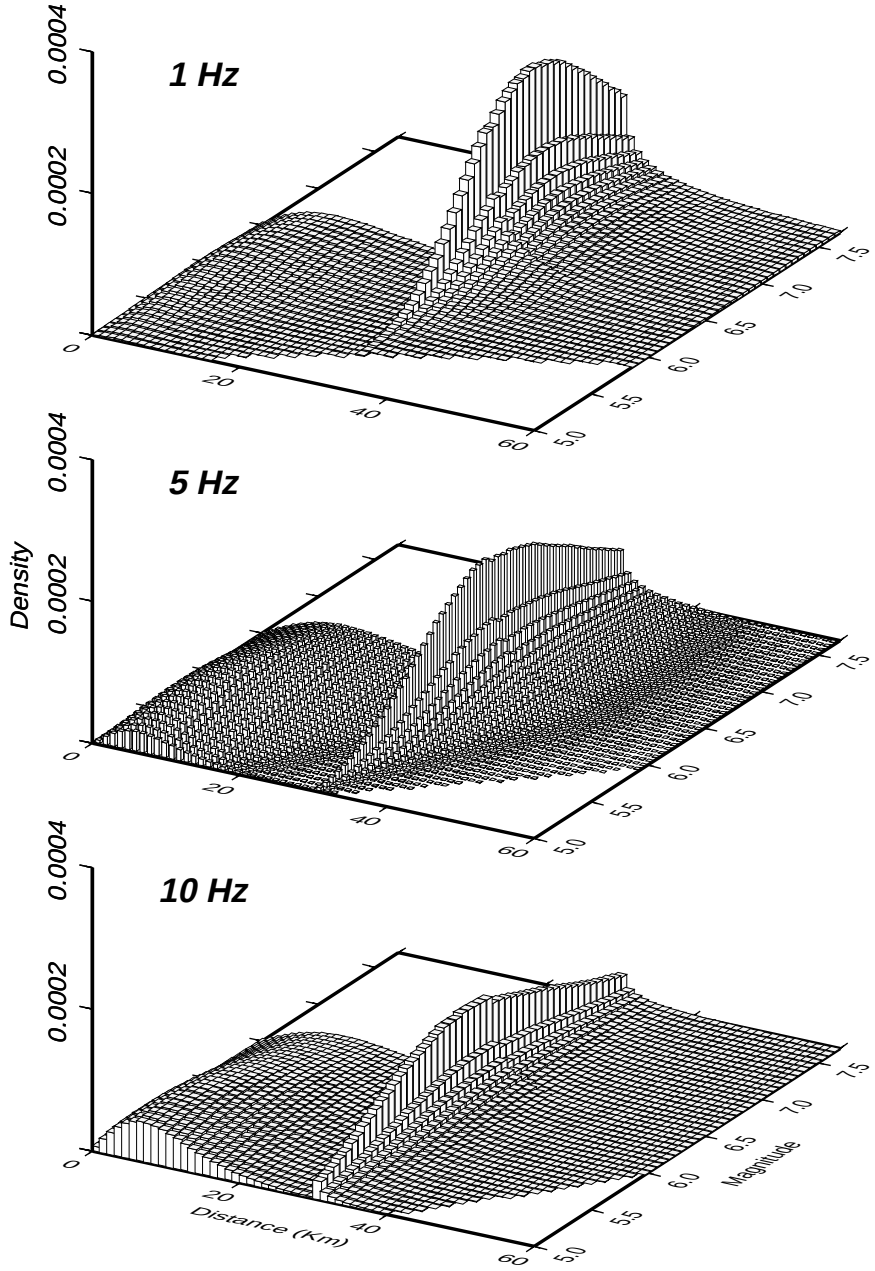

Figure 2.3: Marginal hazard density functions U' for the example discussed in the text. The three functions are for a return period of 500 years, for PSV response. Note that as oscillator frequency increases, the relative contribution to hazard shifts to smaller magnitudes and distances. Modified from Chapman (1995).

Chapter 3: The Use of Elastic Input Energy for Design Event Selection

The probabilistic seismic hazard analysis requires a model from which median estimates of a strong motion parameter can be derived as a function of magnitude, distance and perhaps other variables such as site condition and type of faulting. The model must provide an estimate of the statistical variability of the parameter. Most suitable motion prediction models currently available yield estimates of peak ground motion values or peak response of elastic, single-degree-of-freedom (SDOF) oscillators: e.g., pseudo-relative velocity (PSV) response. Such measures of motion are essentially independent of the duration of the ground motion. As a result, scenario events derived from them do not necessarily represent the optimum events to be used for some types of engineering design studies.

This section of the study examines the potential use of a parameter derived from the elastic input energy spectrum for probabilistic seismic hazard analysis. The input energy reflects the duration of ground shaking directly through time domain integration, and for that reason could potentially provide an improved basis for defining scenario events. A recent comprehensive study by Lawson (1996) developed regression models for both elastic and inelastic input energy spectra, as well as elastic response spectra. The present study uses a similar, but somewhat larger, data set, comprised of western North American strong motion recordings.

The focus of this Chapter is on a comparison of the magnitude and distance dependence of the elastic input energy spectrum with the elastic PSV response spectrum which is commonly used in probabilistic hazard analysis. The objective is to assess the degree to which use of a duration dependent motion parameter changes the results with respect to the type of earthquakes (magnitude and distance) that contribute to hazard at a given probability level. This is done by first developing representative motion prediction models for the two parameters using identical data processing procedures, and then comparing the disaggregated results of simple, but fairly general seismic hazard models.

3.1 Strong Motion Data

The data set used in this study consists of horizontal component recordings from 23 earthquakes in western North America. Table 3.1 lists the earthquakes, along with station names

and site numbers, component azimuth, source to site distance, station coordinates and site classification. The source to station distance adopted for this study is that used by Boore et al., (1993, 1994 and 1997), and is the nearest horizontal distance from the station to the surface projection of the fault rupture. The site classification is that adopted by the NEHRP, (BSSC, 1994; see also Boore et al., 1997) which is defined on the basis of average shear wave velocity in the upper 30 meters (Table 3.2).

Data selection and regression modeling used in this study follows closely the approach developed and used in previous work by Boore et al., (1993, 1994, 1997) and Joyner and Boore (1993, 1994). The data used here were recorded at ground level or in basements of structures of two stories or less, and do not include data from dam or bridge abutments. For 17 of the 23 earthquakes, the data assembled here for analysis is a subset of that used and documented thoroughly by Boore et al. (1993, 1994 and 1997). The remaining data are recordings from the 1994 Northridge shock and from some recent shocks with magnitudes in the range 5.0 to 6.2 (Westmoreland, Morgan Hill, Whittier Narrows, Sierra Madre, and Big Bear).

The sources of strong motion data were the collection of recordings assembled and distributed by NOAA (Earthquake Strong Motion CD-ROM); and the internet websites maintained by the California Division of Mines and Geology strong motion instrumentation program, the U. S. Geological Survey national strong motion program and the Civil Engineering Department, University of Southern California. Table 3.1 identifies the source of the data, along with that organization's site identification number, as appearing in the data file header, if available.

The recordings were selected so as to include the entire S-wavetrain. Recordings that triggered late on the S wave, or those of short duration terminating early in the coda, were not used. The iterative approach described by Campbell (1997) was used to avoid bias due to the effects of non-triggered instruments, in the data sets from some of the more recent shocks. This will be discussed further below.

Corrected accelerogram data provided by the contributing sources comprise a large portion of the assembled data set. However, a sizable fraction of the data was processed by the author for this study. Evenly sampled, uncorrected data were available from the U. S. Geological Survey National Strong Motion Program (NSMP) for the Petrolia, Landers, Big Bear and Northridge earthquakes. Those data were instrument corrected and bandpassed using a 4-pole causal

Butterworth filter with corner frequencies 0.1 and 25 Hz. Unevenly sampled, uncorrected data were available from the University of Southern California (USC) sites for the Whittier Narrows, Sierra Madre, Landers, Big Bear and Northridge earthquakes. Those data were interpolated and sampled evenly using a 0.005 s interval, and instrument corrected. A causal Butterworth bandpass filter with corner frequencies at 0.2 and 25 Hz was then applied. A 6-pole filter was used for the Landers and Big Bear data, whereas a 4-pole filter was used for the Whittier Narrows and Sierra Madre recordings.

In all cases, using corrected data from the contributing sources or data corrected as described above, the recordings were passed through a final filter stage consisting of a 6-pole, causal high-pass Butterworth filter, with corner frequency 0.2 Hz. The filter parameter selections were chosen to insure that low-frequency noise was suppressed. This was verified for all the data by visual inspection of integrated velocity and displacement recordings. The response and energy spectra derived from these data are considered reliable for oscillator frequencies greater than 0.5 Hz.

Site classification according to BSSC (1994) for the recording sites listed in Table 3.1 was obtained from compilations of Boore et al., (1993), Harmsen (1997) and Boore et al., (1997). Source to recording site distances for all earthquakes occurring prior to 1981, as well as for the Loma Prieta and Petrolia earthquakes, are taken from Boore et al., (1993, 1997). Site distances for the Westmoreland earthquake were calculated using the aftershock distribution as given by Sharp et al. (1986). Distances for the Morgan Hill earthquake were calculated from the aftershock distribution summarized by Cockerham and Eaton (1987). The aftershock distributions given by Hauksson (1994) were used to calculate the site distances for the Whittier Narrows and Sierra Madre earthquakes. Distances for the Landers and Big Bear earthquakes were derived from the aftershock distributions and the fault model of Wald and Heaton (1994). Distances for the Northridge earthquake were derived using the rupture model of Wald et al., (1996).

Figure 3.1 shows the distribution of data in terms of magnitude, distance and site classification. Site classes A and B (Table 3.2) are combined for analysis, because so few data are available.

3.2 Response Parameters

The emphasis of this study in on comparing the distance and magnitude dependence of maximum elastic oscillator response and of input energy. Regression analysis is performed on peak horizontal ground acceleration (PGA), peak horizontal ground velocity (PGV), elastic oscillator pseudo-relative velocity response (PSV) and a parameter derived from the absolute input energy for elastic oscillators. The regression models are derived for a randomly oriented horizontal component, using the geometric mean of the two horizontal components.

The values of PGA and PGV used in this study are those values obtained from the corrected acceleration and integrated corrected acceleration recordings, following filtering as described above. Note that a small difference exists in the values of those parameters used in regression and the values of the original recordings.

The algorithm of Nigam and Jennings (1969) was used to calculate the elastic oscillator response time series necessary for construction of PSV and energy spectra.

3.2.1 Input Energy

Following Uang and Bertero (1990), the equation of motion of a damped SDOF system is

$$m\,(\ddot{x}_g + \ddot{x}) + c\,\dot{x} + f = 0 \qquad (3.1)$$

Here, x_g is the displacement of the ground, and x is the relative displacement of the mass with respect to the ground, c is the damping coefficient and f is the restoring force. The equation of motion of an equivalent system with fixed base, acted upon by a force $-m\,\ddot{x}_g$ is given by

$$m\,\ddot{x} + c\,\dot{x} + f = -m\ddot{x}_g \,. \qquad (3.2)$$

Uang and Bertero (1990) show that the equivalent representations of the dynamic system lead to two definitions of input energy. Integrating Equation 3.1 with respect to x leads to

$$m\,\dot{x}_t^2/2 + \int c\dot{x}\,dx + \int f\,dx = \int m\,\ddot{x}_t\,dx_g \,, \qquad (3.3)$$

where $x_t = x_g + x$, is the total or absolute displacement. Integration of Equation 3.2 with respect to x leads to

$$m\dot{x}^2/2 + \int c\dot{x}\,dx + \int f\,dx = -\int m\ddot{x}_g\,dx \quad . \qquad (3.4)$$

The RHS of Equation 3.3 is known as the absolute input energy E_a, and can also be expressed as

$$E_a = \int m\ddot{x}_t\,dx_g = \int m\ddot{x}_t\dot{x}_g\,dt = \int m(\ddot{x}+\ddot{x}_g)\dot{x}_g\,dt \qquad (3.5)$$

The RHS of Equation 3.4 is the relative input energy E_r, which can be written as

$$E_r = -\int m\ddot{x}_g\,dx = -\int m\ddot{x}_g\dot{x}dt \; . \qquad (3.6)$$

Note that the damping and strain energy terms are the same in Equations 3.3 and 3.4, and that the distinction between "absolute" and "relative" applies to the input and kinetic energies. The absolute input energy is the work done by the total force applied to the base of the structure. The relative input energy is the work done by an equivalent lateral force on a fixed base system, and neglects the effects of rigid body translation (Uang and Bertero, 1990).

Let V_{ea} and V_{er} be the maximum values of $(2E_a/m)^{1/2}$ and $(2E_r/m)^{1/2}$, respectively. The energy-based equivalent velocities V_{ea} and V_{er} are asymptotic to the peak ground velocity for high and low oscillator frequencies, respectively. V_{ea} and V_{er} are nearly equivalent for oscillator frequencies within the band of appreciable PSV response, corresponding to that part of the Fourier spectrum of the ground acceleration with significant amplitudes. They diverge outside that frequency band. At oscillator frequencies low compared to the dominant frequencies of the ground acceleration, V_{ea} approaches zero, whereas V_{er} is asymptotic to the maximum ground velocity. At high oscillator frequencies, V_{er} approaches zero, whereas V_{ea} is asymptotic to the maximum ground velocity. Regardless of oscillator frequency, $E_a = E_r$ if both are evaluated at the end of the ground motion episode. However, the maximum values of E_a and E_r, and the parameter V_{ea} of interest here, do not generally occur at the end of the ground motion episode. For example, in the case of high frequency oscillators, V_{ea} occurs near the time of the maximum ground velocity, and is larger than V_{er}.

Figure 3.2 illustrates the relationship between the energy parameters V_{ea}, V_{er} and the PSV spectrum.

3.3 Regression Analysis

The following regression model (Boore et al., 1993) is fitted to the PSV and V_{ea} data sets, and to the peak ground acceleration (PGA) and velocity (PGV) data.

$$\text{Log}_{10}\, Y = a + b(M-6) + c(M-6)^2 + d \log (r^2 + h^2)^{1/2} + e\, G_1 + f\, G_2 + \varepsilon. \quad (3.7)$$

Here, Y is the response variable (the geometric mean of the two horizontal components), expressed in units of centimeters and seconds, M is moment magnitude, r is the horizontal distance, in km, to the nearest surface projection of the fault rupture, and G_1 and G_2 are indicator variables for site classifications C and D (e.g.: G_1=1 for class C sites, 0 otherwise, G_2 = 1 for class D sites, 0 otherwise). The unknowns a,b,c,d,h,e,f and the variance σ^2 of random error ε are determined using the two-step regression procedure of Joyner and Boore (1993, 1994).

The normally distributed error term ε has zero mean and standard deviation σ composed of two components, such that $\sigma^2 = \sigma_r^2 + \sigma_e^2$. The variance σ_r^2 is associated with the first stage of the regression wherein the unknowns d, h, e and f are estimated, along with "amplitude factors" for each of the earthquakes. The variance σ_e^2 is that associated with the second stage regression wherein the amplitude factors are regressed against magnitude. For the model of a randomly oriented horizontal component, the response Y is the geometric mean of the two horizontal components, and the estimate of σ_r^2 must be increased to account for the variance associated with choosing one of the components randomly (Boore et al., 1993).

3.3.1 Peak Acceleration, Velocity

To avoid bias due to non-triggered stations, the PGA regression model was developed iteratively, as described by Campbell (1997). In the first step, the entire assembled data set was used to determine a set of minimum distances at which the 16th percentile values of the model is less than 0.02 g, corresponding to a 0.01g vertical component trigger threshold. These distances are functions of magnitude and site condition. Next, corresponding data points at larger distances were deleted and the regression was repeated. One iteration was sufficient to eliminate potentially biased data points, based on the 16th percentile criterion. The remaining data (Table 3.1) were

then used in all further regressions of PGA, PGV, PSV and the energy-based equivalent velocity V_{ea}. Figure 3.3 plots the minimum cutoff distances as a function of magnitude and site class.

Table 3.3 lists the results of the regression analysis for peak ground acceleration (PGA) and velocity (PGV). Figure 3.4 plots the models for the randomly oriented horizontal component, for the combined site classes A & B, as a function of magnitude and distance. Figures 3.5 and 3.6 show the regression residuals as functions of distance and magnitude. Figure 3.4 suggests that PGA undergoes saturation for M>6.5. Also, the effect of site classification is larger for PGV than for PGA. Regression coefficients e and f for PGA correspond to amplification factors of 1.40 and 1.55 for site classes C and D, respectively. These amplification factors have values of 1.53 and 2.00, respectively, for PGV. Figures 3.5 and 3.6 show that Equation 3.7 does a good job overall of fitting the PGA and PGV data, with no obvious non-normal magnitude or distance dependent trends apparent in the residual plots. The data scatter for PGV is somewhat larger than for PGA.

3.3.2 PSV and Energy Spectra

Tables 3.4 through 3.6 list regression results for PSV for 3 values of damping (2%, 5% and 10% critical). Tables 3.7 through 3.9 list corresponding results for V_{ea}. Figure 3.7 shows residuals versus distance and magnitude for oscillator frequencies 1 Hz and 5 Hz. Figure 3.8 shows corresponding residual plots for Vea.

The residuals show no obvious magnitude or distance dependent trends, and it is apparent that the regression model Equation 3.7 is equally appropriate for PSV and V_{ea}. Figures 3.7 and 3.8 are representative of results obtained for other frequency and damping values.

Figure 3.9 compares the regression coefficients versus frequency for V_{ea} and PSV at 5% damping. The linear magnitude coefficient "b" is significantly larger (more positive) for the energy-based parameter V_{ea} than for PSV, at the higher frequencies, indicating a stronger high-frequency scaling of V_{ea} with magnitude. The distance coefficient "d" is also more positive for V_{ea}, indicating a tendency for less distance attenuation of the parameter, compared to PSV, at all frequencies. The parameter "h", which functions as a pseudo-focal depth term, is nearly the same for V_{ea} and PSV for frequencies less than about 3 Hz. At higher frequencies, h for PSV exceeds that for V_{ea}. The site class coefficients "e" and "f" are very similar for V_{ea} and PSV. In both cases, the effect of site class is most important at the lower frequencies. The effects of site class

are unresolved by the regression analysis at frequencies greater than 5 Hz. Finally, the standard deviation of the regression, σ, generally decreases with increasing oscillator frequency, and is uniformly smaller for V_{ea} than for PSV, as can be seen from a comparison of Figures 3.7 and 3.8. The results just described are much the same for the 2% and 10% damped oscillators.

The relative magnitude and distance dependence of PSV and V_{ea} is illustrated in Figure 3.10 which plots the ratio V_{ea}/PSV derived from the regression models, versus distance for discrete values of magnitude and oscillator frequency. The ratio V_{ea}/PSV is an increasing function of magnitude and distance, for distances greater than about 15 km. This means that V_{ea} increases more rapidly with increasing earthquake magnitude, and decays more slowly at larger distances. However, the effect is strongly dependent upon oscillator frequency. The difference between magnitude and distance scaling of V_{ea} and PSV is largest at the highest oscillator frequency, and is negligible for oscillator frequencies less than about 2 Hz.

Figure 3.11 summarizes some important differences between PSV and V_{ea}, by plotting both spectra for several magnitudes at 5 and 50 km distance. At low frequencies (less that approximately 2 Hz) V_{ea} and PSV spectra exhibit similar magnitude scaling. At the higher frequencies the PSV spectra exhibit near saturation for M>6.5, whereas the V_{ea} spectra continue to increase with increasing earthquake magnitude.

3.4 Implications for Seismic Hazard Assessment

The identification of the events, in terms of magnitude and distance, that contribute most to seismic hazard for a given probability of exceedance has practical application. It can serve as a guide for defining scenarios and design earthquakes for engineering problems, particularly those involving dynamic analysis using ground motion time series. The information can be obtained by "disaggregating" the results of a seismic hazard calculation. The V_{ea} spectrum involves the effects of ground motion amplitude and duration, and may prove to be more useful for these types of problems than the elastic response spectrum (e.g., PSV). In the following, we examine differences in the results of simple hazard calculations using the two different motion parameters.

We will examine first the elemental model of a point source for earthquakes. We assume the following recurrence model: Log n = 2.8 - 0.8 m. We assume a truncated exponential form for

$f_M(m)$, with lower and upper magnitude bounds at $m^-=5.0$ and $m^+=7.7$, and $\alpha = 0.0626$ events/year.

Figure 3.12 shows the marginal density functions U'(m,r | g) for several frequencies, for two cases: point sources at 10 and 60 km, and return periods 2500 and 500 years, respectively. As expected from the similarity of magnitude scaling in the regression models, there is little difference in the density functions for the low frequency oscillators (e.g., 0.5 and 1.0 Hz). However, for 2.0 Hz, $\underline{m}'$ for V_{ea} is approximately 0.2 magnitude units larger than $\underline{m}'$ for PSV. This difference increases to approximately 0.6 units for the 6.7 Hz oscillator. Similar differences occur for $\underline{m}$. Table 3.10 summarizes the values of g, ($\underline{m}'$, $\underline{r}'$) and the β-point ($\underline{m}$, $\underline{r}$, $\underline{\varepsilon}$) for the examples shown in Figure 3.12. It is apparent that differences in magnitude scaling of V_{ea} and PSV result in substantial differences of the derived modal earthquake magnitudes of the U and U' density distributions, at higher frequencies. The modal magnitudes for V_{ea} (either $\underline{m}'$ or $\underline{m}$) are larger than those for PSV, and tend to decrease less rapidly (i.e., vary less) with increasing oscillator frequency. In this example, design earthquakes based on $\underline{m}$ would, in the case of V_{ea}, focus on earthquakes with magnitudes in the relatively narrow range 6.81 to 7.03 for the 60 km, 2500 year scenario, whereas if the calculations are done using PSV, a much wider range of magnitudes (6.27 to 7.08) is indicated for the frequency band 0.5 to 6.67 Hz. For the higher frequency oscillators, it is clear that the use of V_{ea} itends to "focus" the contribution to hazard at larger magnitudes.

Another simple, but somewhat more realistic hypothetical seismic hazard model is suggested by Figure 2.1. As was done in the example calculations of Chapter 2, we again assume two independent sources for earthquakes, involving a "fault" (a line source along which earthquakes occur as point sources with uniform probability), and a less active "background" source area. All hazard model parameters are as in the example discussed previously (Equations 2.10, 2.11 and 2.12).

Using this model, for NEHRP combined site classes A&B, we calculate 500 year uniform hazard spectra for PSV and V_{ea}, and determine corresponding values for ($\underline{m}'$,$\underline{r}'$) and ($\underline{m}$,$\underline{r}$,$\underline{\varepsilon}$) for each source. Table 3.11 contains the results of the calculation. Figure 3.13 shows the marginal density functions U'(m,r | x) for five oscillator frequencies (5% damping), along with the percentage contribution to total hazard by the "background" and "fault" sources.

The results of the exercise involving the background+fault model are consistent with those of the point source models, and reinforce the observation that larger magnitude earthquakes consistently contribute more to the seismic hazard determined using elastic input energy as the basis for the assessment, rather than the elastic response spectrum. For the line source, the modal magnitudes $\underline{m}$ based on V_{ea} range from 6.73 to 7.08 for frequencies between 0.5 and 6.7 Hz, whereas the modal magnitudes for the PSV calculation range from 6.38 to 6.98. The similarity of results for the line source with those of the point source model is expected due to the peaked nature of the $f_R(r)$ probability density function for the line source at r=30 km. The difference between V_{ea} and PSV results for the background source are smaller, but still significant: $\underline{m}$ for V_{ea} exceeds $\underline{m}$ for PSV by approximately 0.2 to 0.3 magnitude units for frequencies greater than 1.0 to 2.0 Hz. Here, the choice of motion parameter has a substantial impact upon the perceived source of the seismic hazard. In comparing the results of the V_{ea} calculation with those using PSV, the contribution by the background to total hazard at 2 Hz, 3 Hz and 6.7 Hz decreases by 10 to 20 percent, while that of the "fault" increases a corresponding amount. This has implications for the problem of design earthquake selection. In this simple example, use of V_{ea} puts more emphasis upon a scenario involving a larger magnitude shock associated with the "fault" source, than would be the case if PSV where used in the hazard calculation.

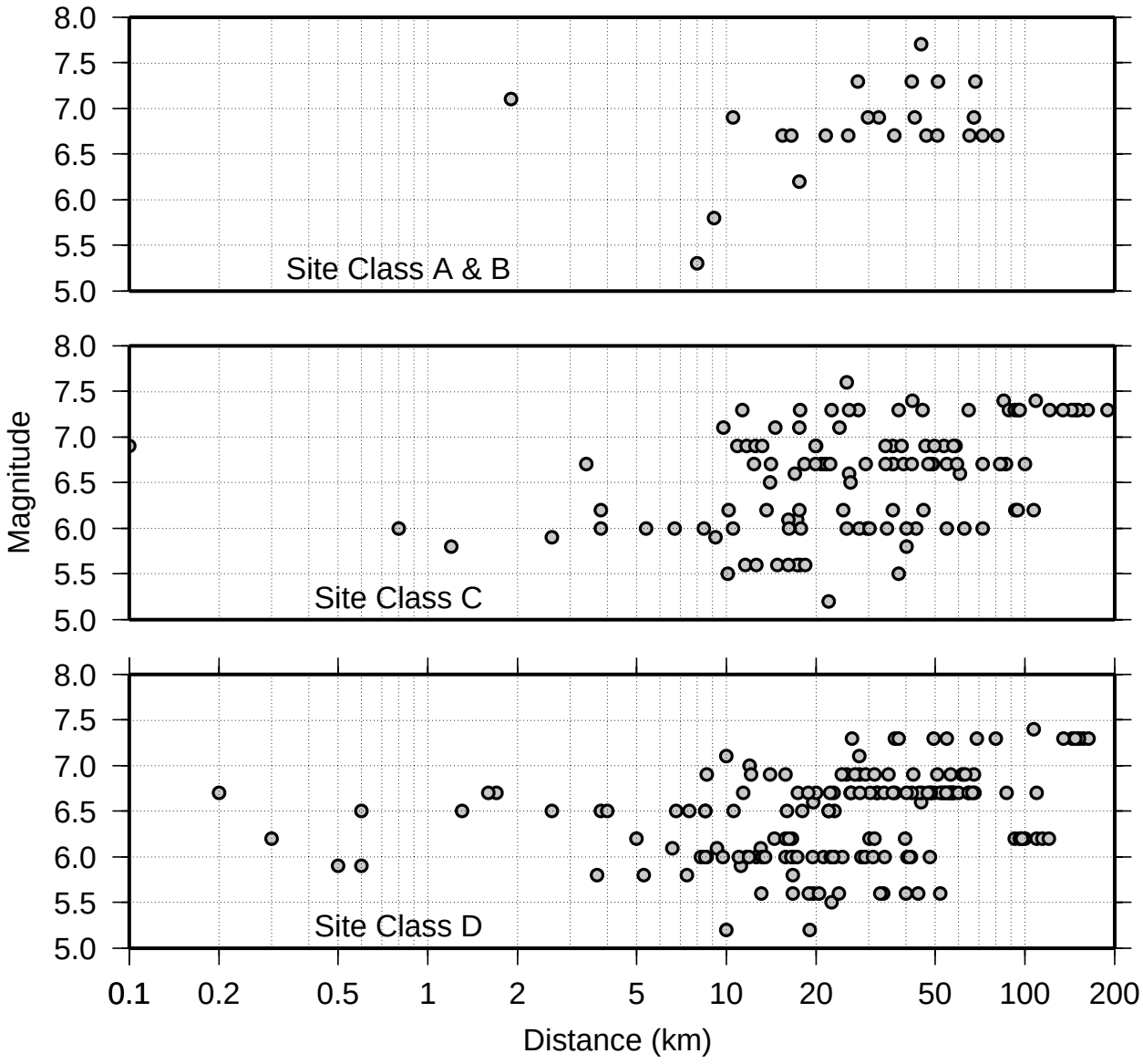

Figure 3.1: Distribution of data in terms of magnitude, distance and site classification, Top: NEHRP site classes A and B, combined, n=24. Middle: site Class C, n=116. Bottom: site class D, n=164.

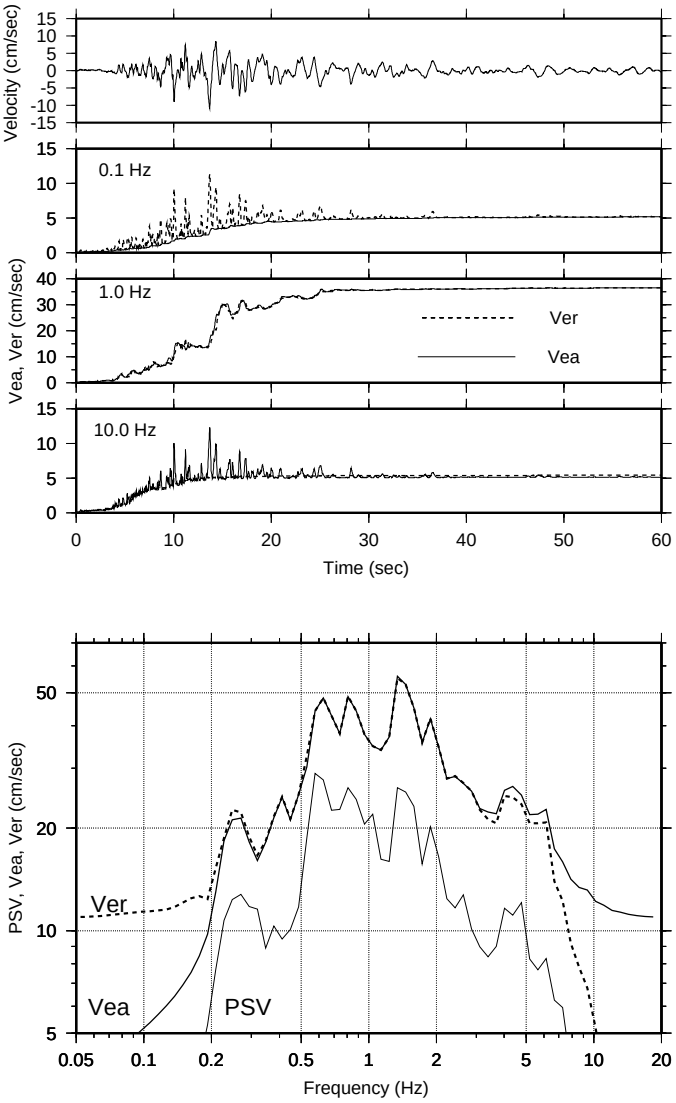

Figure 3.2: Relationships between PSV and energy based equivalent velocities Vea and Ver, using the east-west component of motion at the Alhambra station from the Northridge earthquake. Top: ground velocity. Middle: time series for Vea and Ver for 5 percent damped, elastic oscillators of frequency 0.1, 1.0 and 10.0 Hz. Bottom: corresponding PSV, Vea and Ver spectra.

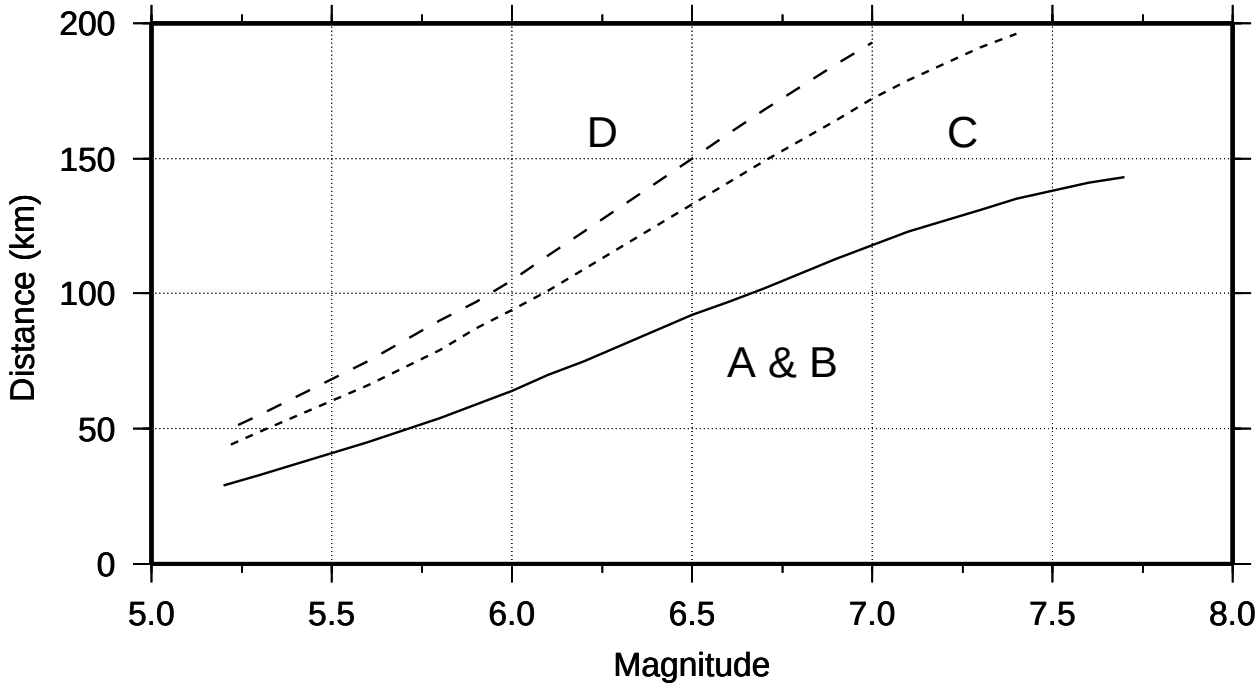

Figure 3.3: Data selection cutoff distance versus magnitude and site class.

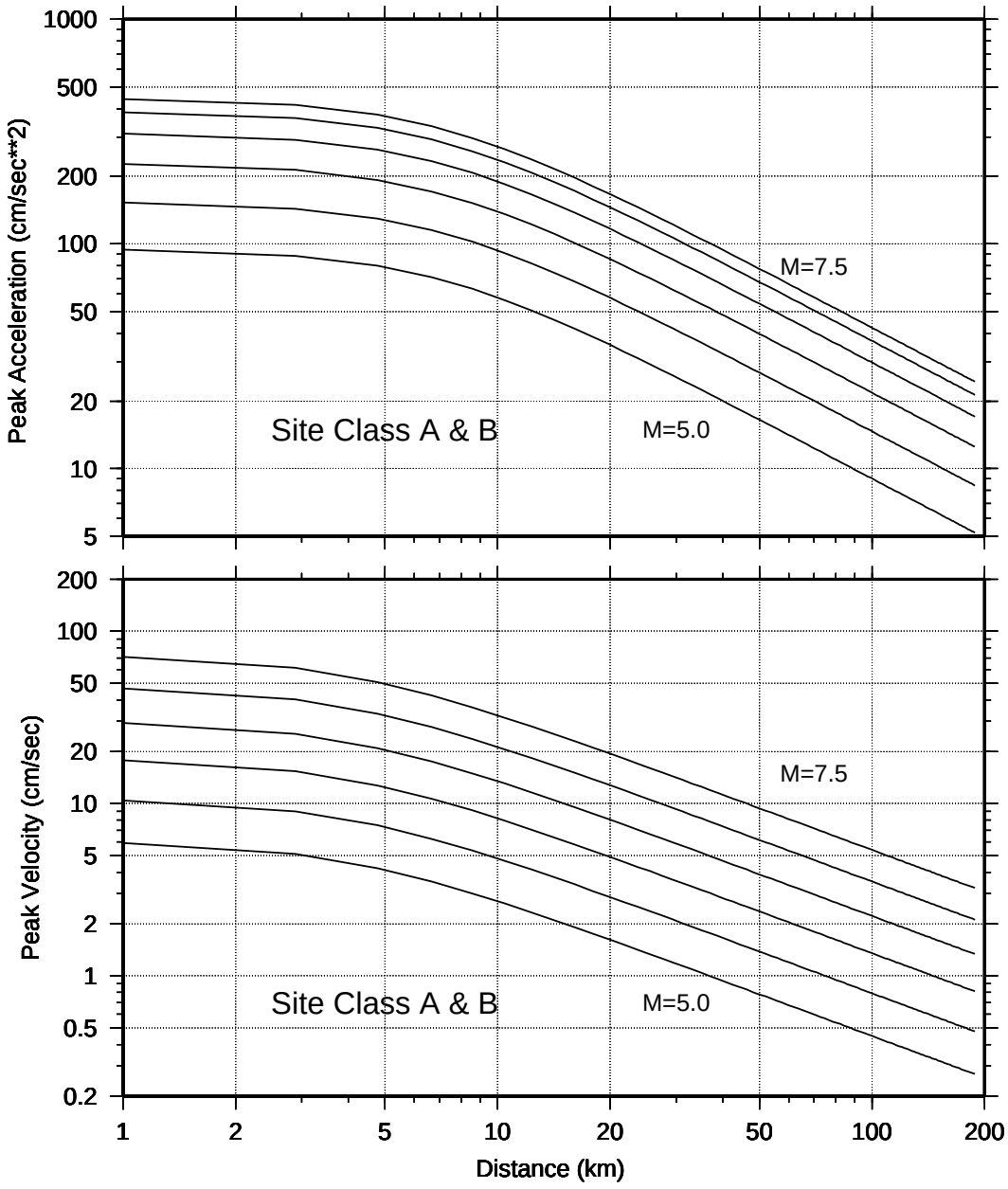

Figure 3.4: Top: peak ground acceleration for a randomly oriented horizontal component, NEHRP site classes A and B, combined. Curves are plotted for moment magnitudes 5.0, 5.5, 6.0, 6.5, 7.0 and 7.5. Site class C and D models exceed those plotted by factors of 1.40 and 1.55, respectively. Bottom: peak ground velocity. Site class C and D models exceed those plotted by factors 1.53 and 2.00, respectively.

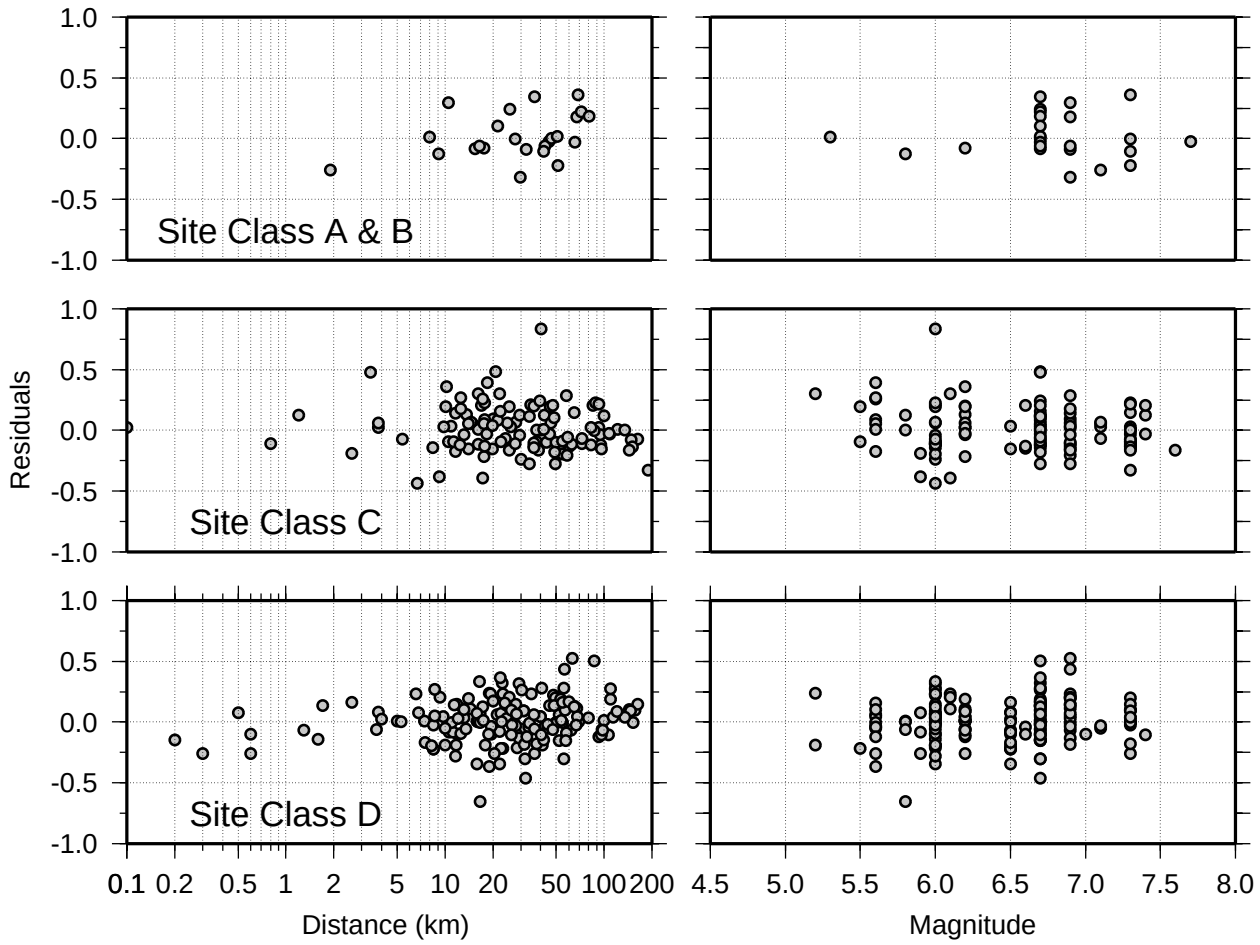

Figure 3.5: Regression residuals for peak ground acceleration, randomly oriented horizontal component.

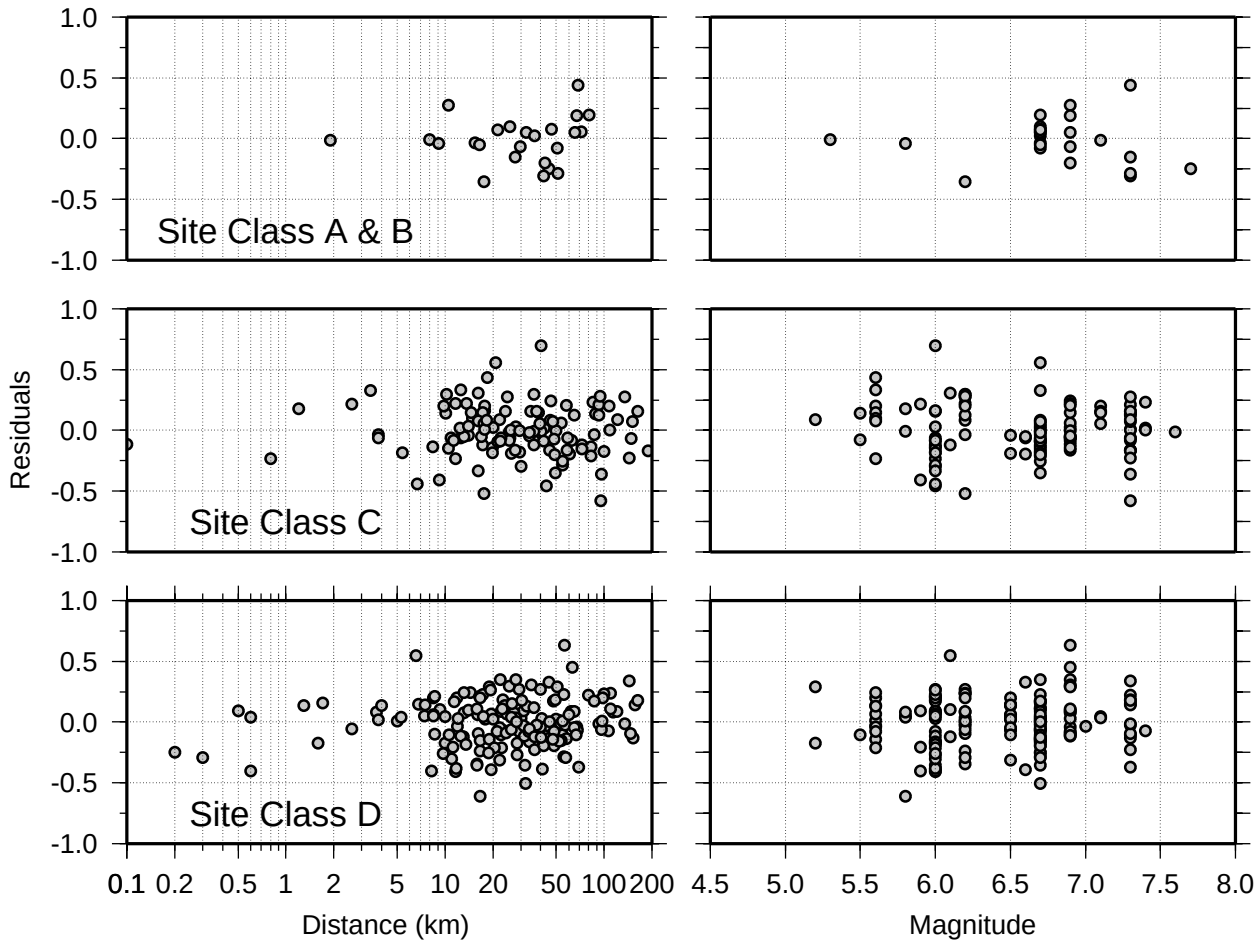

Figure 3.6: Regression residuals for peak ground velocity, randomly oriented horizontal component.

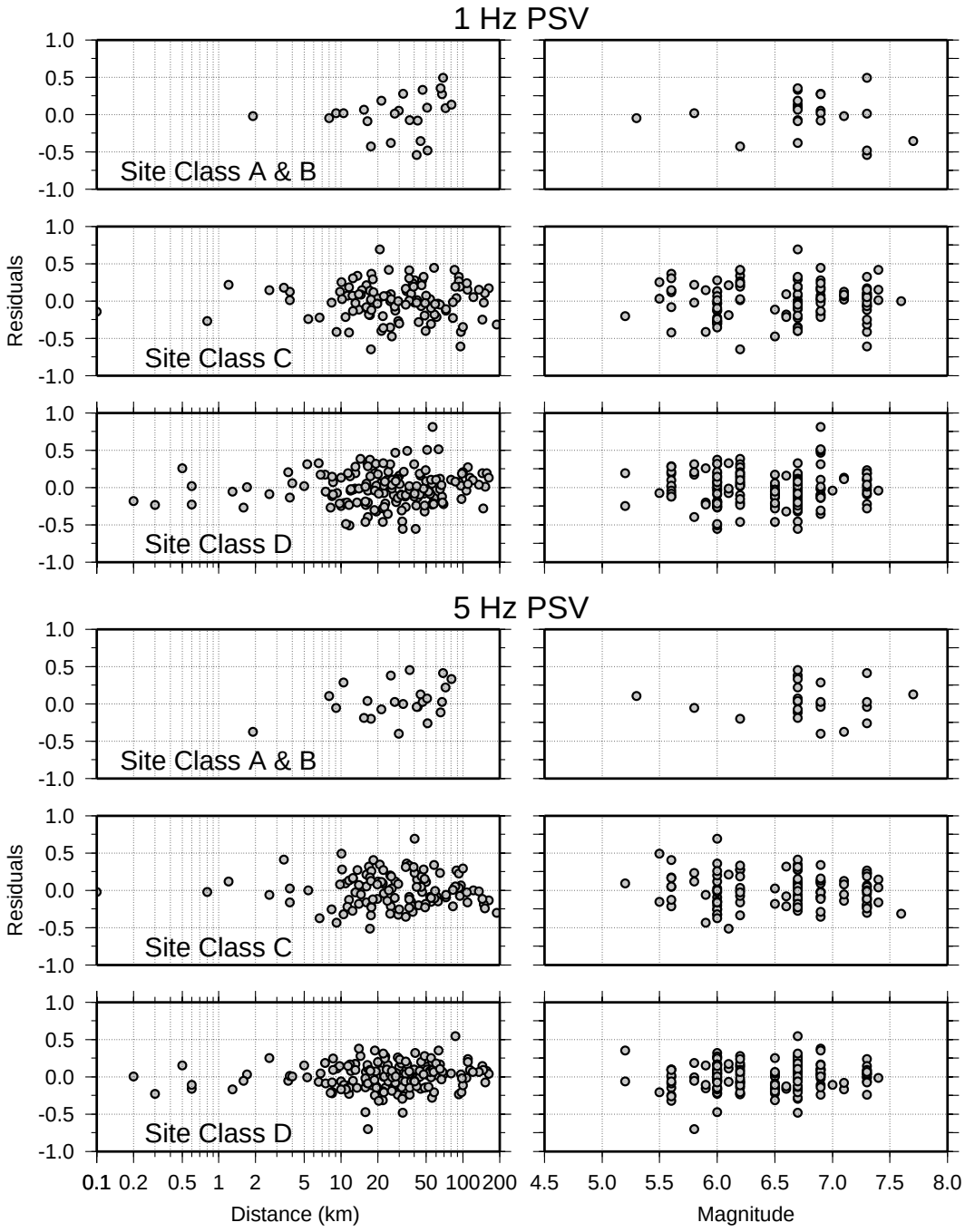

Figure 3.7: PSV regression residuals for 1 Hz (upper) and 5 Hz (lower) oscillators, (5 percent damping) randomly oriented horizontal component.

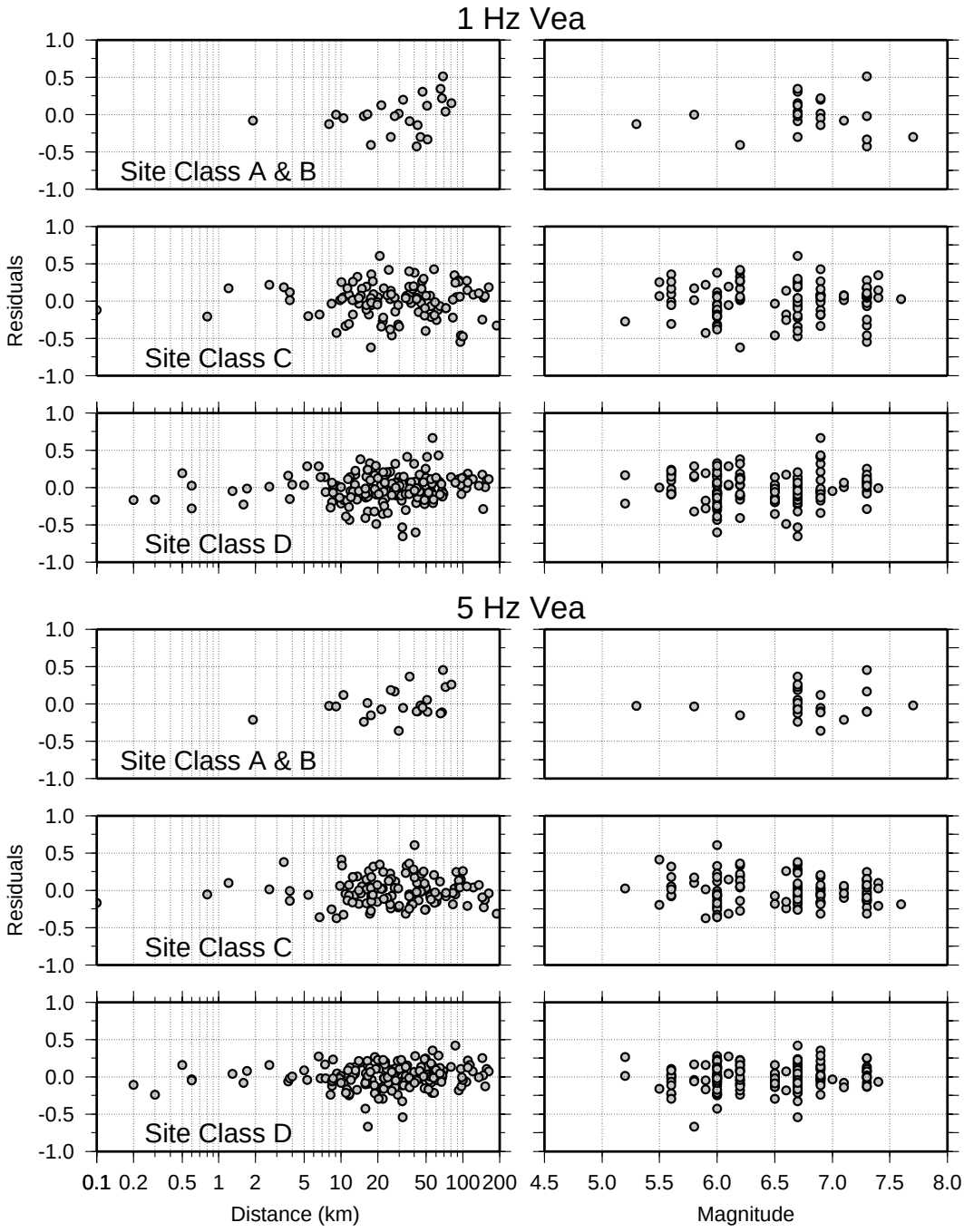

Figure 3.8: Vea regression residuals for 1 Hz (upper) and 5 Hz (lower) oscillators, (5 percent damping) randomly oriented horizontal component.

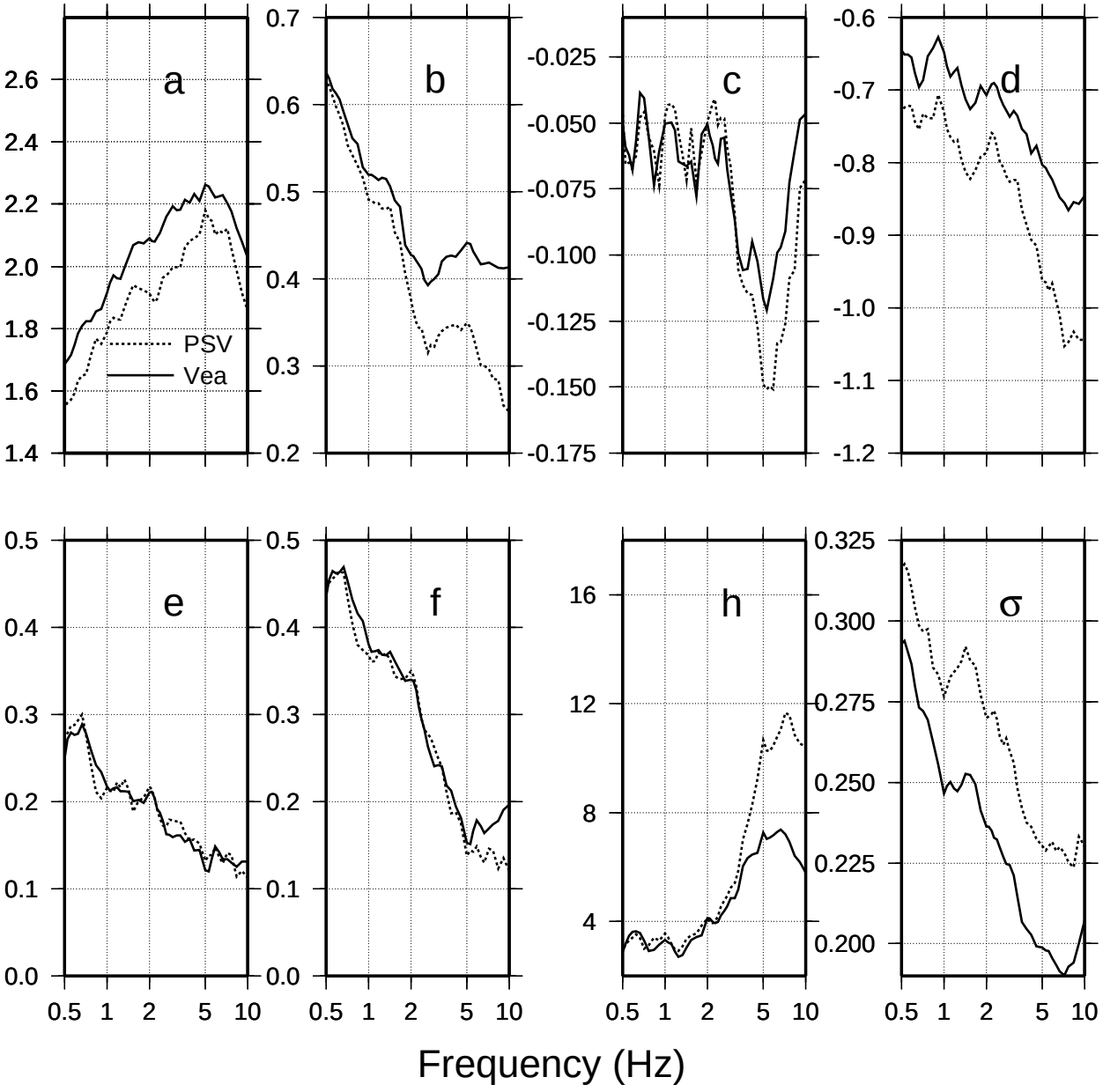

Figure 3.9: Estimated regression model coefficients (Equation 3.7), for PSV and Vea, as functions of oscillator frequency (5 percent damping).

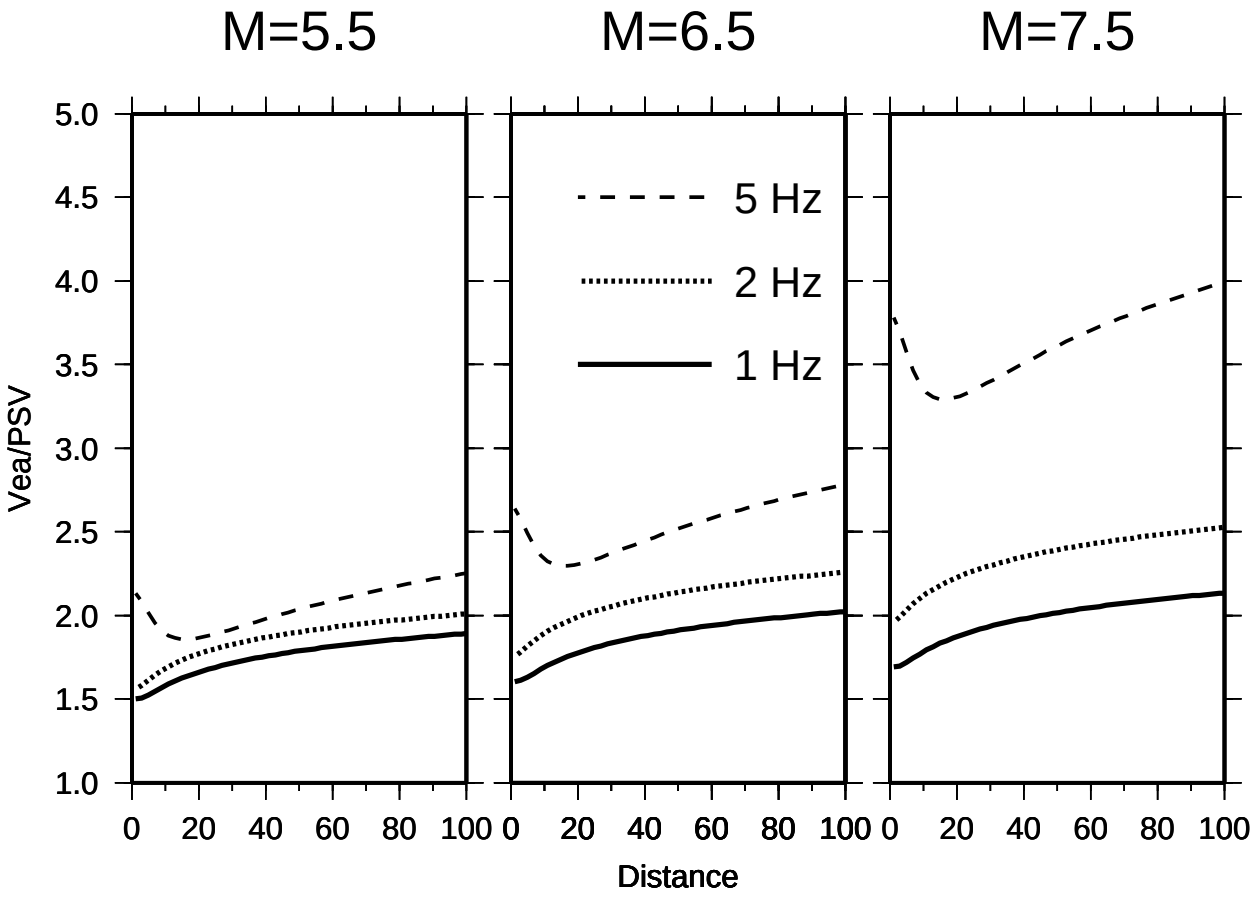

Figure 3.10: The ratio Vea/PSV versus distance for M=5.5 (left), M=6.5 (center) and M=7.5 (right). Results for 3 different oscillator frequencies are shown, for 5 percent damping and a randomly oriented horizontal component, NEHRP site class A and B, combined.

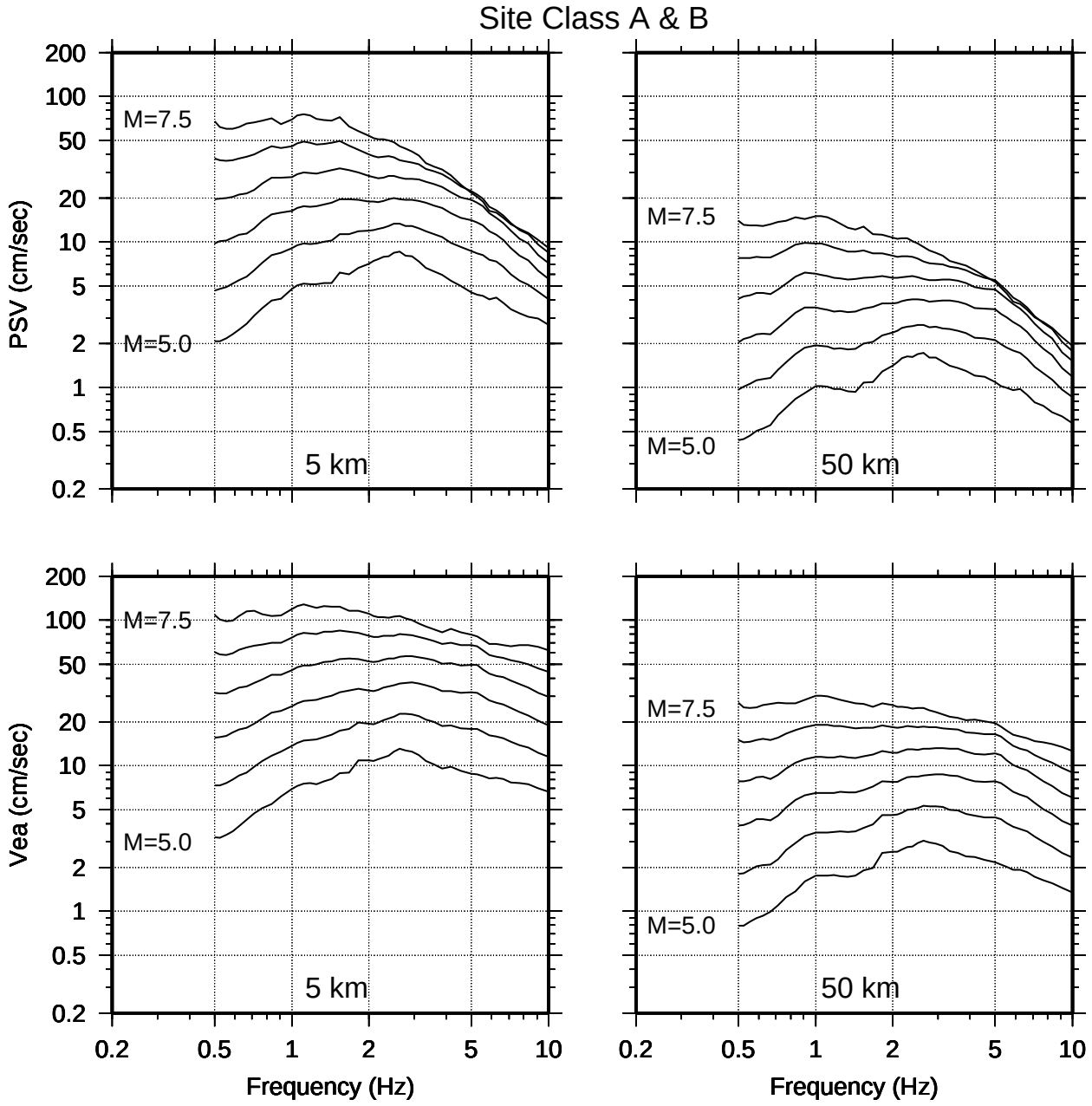

Figure 3.11: PSV (upper) and Vea (lower) spectra for site class A and B, combined. Spectra are for 5 percent damping, and a randomly oriented horizontal component, for 5 and 50 km distance.

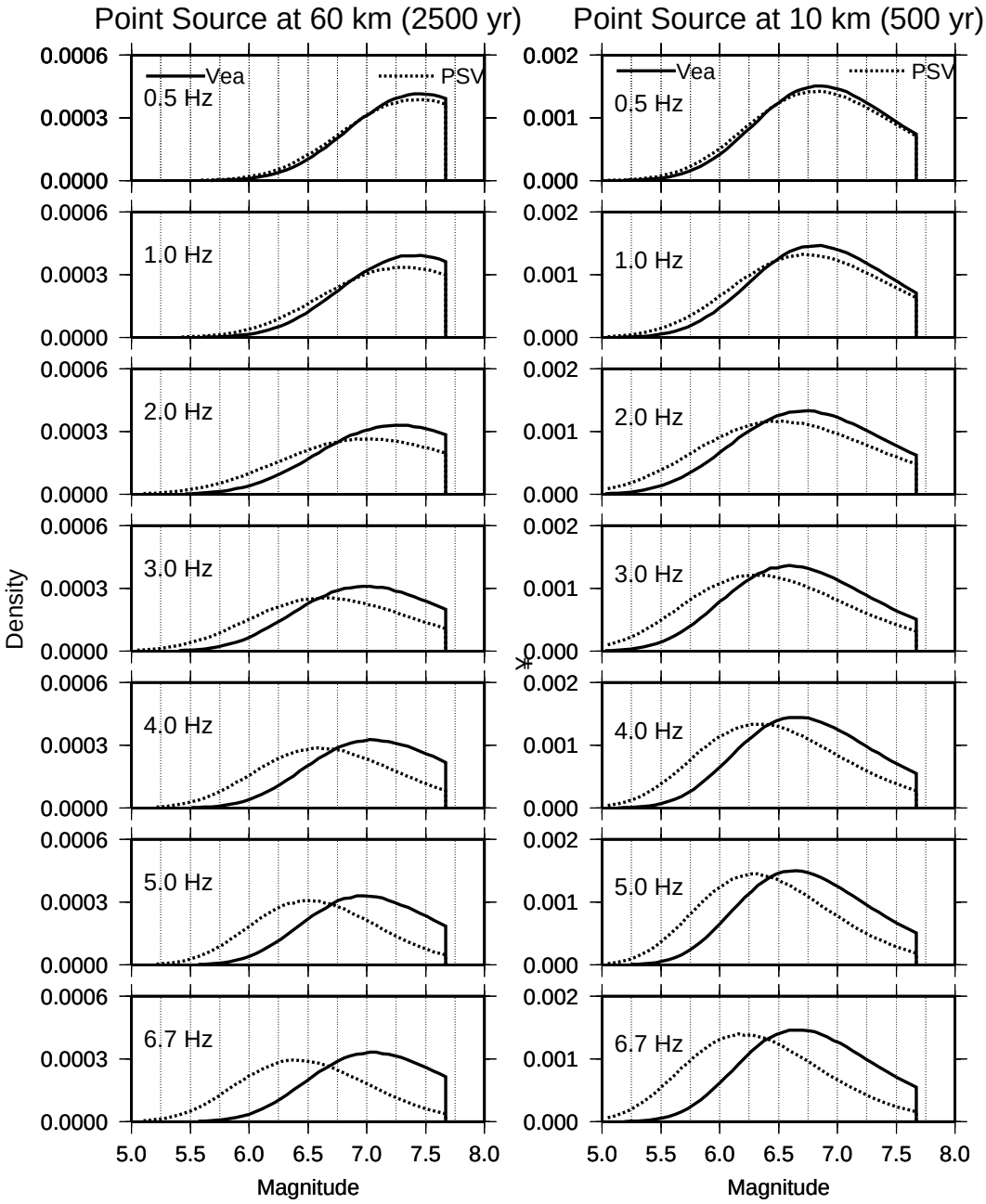

Figure 3.12: Marginal density functions U' for two examples involving point sources for earthquakes at 60 km (left) and 10 km (right). Refer to Table 3.10 for values of the modal magnitudes and motion values.

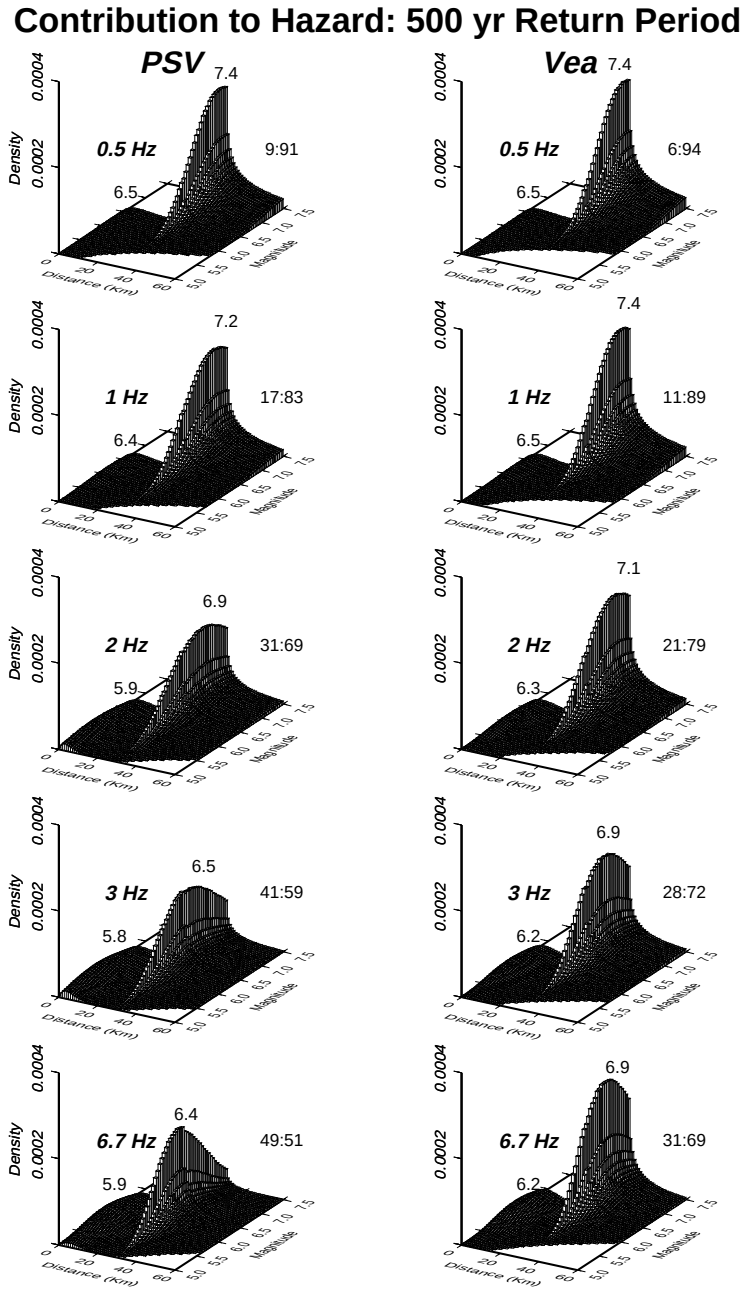

Figure 3.13: Marginal density functions U' for the example calculation in the text. The modal magnitudes are indicated for each source, as are the relative contributions, in percent of the total hazard, of each source. The calculations are for a 500 year return period, and combined A and B site class. Refer to Table 3.11 for values of the marginal and joint modal events.

Table 3.1

Strong Motion Recordings Used in Regression Analysis

Earthquake	Site Name	Site Number*	Az1	Az2	Dist (km)	Lat. N	Lon. W	Class
Imperial Valley May 19, 1940 M=7.0	El Centro #9	(ct 117)	180	270	12.0	32.795	115.549	c
Kern County July 21, 1952 M=7.4	Taft Lincoln sch	(ct 95)	21	111	42.0	35.150	119.450	b
	Santa Barbara CH	(ct 283)	42	132	85.0	34.424	119.701	b
	Cal Tech Athena.	(ct 475)	180	270	109.0	34.139	118.121	b
	Hollywood St. Bld.	(ct 135)	180	90	107.0	34.083	118.333	c
Daly City Mar. 22, 1957 M=5.3	Golden Gate Park	(ct 077)	10	100	8.0	37.667	122.483	a
Parkfield June 28, 1966 M=6.1	Cholame Shandon #2	(ct 13)	65	---	6.6	35.731	120.286	c
	Cholame Shandon #5	(ct 14)	355	85	9.3	35.700	120.328	c
	Cholame Shandon #8	(ct 15)	50	320	13.0	35.671	120.360	c
	Cholame Shandon #12	(ct 16)	50	320	17.3	35.636	120.403	b
	Cholame Shandon Tmblor #2	(ct 97)	295	205	16.1	35.752	120.264	b
Borrego Mtn. April 9, 1968 M=6.6	El Centro Array #9	(ct 117)	90	270	45.0	32.794	115.54	c
San Fernando Feb. 9, 1971 M=6.6	Caltech Athenaeum	(ct 475)	0	90	25.7	34.139	118.121	b
	Lake Hughes Sta. 4	(ct 126)	111	201	19.6	34.642	118.480	c
	Lake Hughes Sta. 12	(ct 128)	21	249	17.0	34.572	118.560	b
	Wrightwood	(ct 290)	25	115	60.7	34.361	117.633	b
Sitka July 30, 1972 M=7.7	Sitka magnetic observatory	(2714)	180	90	45.0	57.060	135.320	a
Managua Dec. 23, 1972 M=6.2	ESSO Refinery	----	180	90	5.0	12.145	86.322	c
Hollister Nov. 28, 1974 M=5.2	San Juan Buatista	---	237	33	10.0	36.860	121.540	c
	Hollister City Hall annex	(usgs 1575)	181	271	19.0	36.851	121.402	c
	Gilroy -Gavilan College	(cdmg 47379)	247	157	22.0	36.973	121.572	b
St. Elias Feb. 28, 1979 M=7.6	Icy Bay, Gulf Timber Co.	(2734)	180	90	25.4	59.968	141.643	b

Coyote Lake	Gilroy Array 1	(cdmg 47379)	320	230	9.1	36.973	121.572	a
Aug. 6, 1979	Gilroy Array 2	(cdmg 47380)	140	50	7.4	36.982	121.556	c
M=5.8	Gilroy Array 3	(cdmg 47381)	140	50	5.3	36.987	121.536	c
	Gilroy Array 4	(cdmg 57382)	360	270	3.7	36.005	121.522	c
	Gilroy Array 6	(cdmg 57383)	320	230	1.2	37.026	121.484	b
Imperial Valley	El Centro Array #7	(usgs 5028)	230	140	0.6	32.829	115.504	c
Oct. 15, 1979	El Centro Array #6	(usgs 5158)	230	140	1.3	32.839	115.487	c
M=6.5	El Centro Bonds Corner	(usgs 5054)	230	140	2.6	32.693	115.338	c
	El Centro Array #8	--	230	140	3.8	32.810	115.530	c
	El Centro Array #5	(usgs 0952)	230	140	4.0	32.855	115.466	c
	El Centro Array #4	(usgs 0955)	230	140	6.8	32.864	115.432	c
	Brawley	(usgs 5060)	315	225	8.5	32.991	115.512	c
	El Centro Array #10	(usgs 0412)	50	320	8.5	32.780	115.567	c
	Parachute Test Site	(usgs 5051)	315	225	14. 0	32.929	115.699	b
	El Centro Array #2	(usgs 5115)	230	140	16.0	32.916	115.366	c
	El Centro Array #12	(usgs 0931)	230	140	18.0	32.718	115.637	c
	Calipatria	(usgs 5061)	315	225	23.0	33.130	115.520	c
	El Centro Array #13	(usgs 5059)	230	140	22.0	32.709	115.683	c
	El Centro Array #1	(usgs 5056)	230	140	22.0	32.960	115.319	c
	Superstition Mtn	(usgs 0286)	135	45	26.0	32.955	115.823	b
	Holtville	(usgs 5055)	315	225	7.5	32.812	115.377	c
	Calexico	(usgs 5053)	315	225	10.6	32.669	115.492	c
Livermore	San Ramon	(cdmg 0134)	70	340	16.7	37.780	121.980	c
Jan. 24, 1980	APEEL 3E	(cdmg 0219)	146	236	40.3	37.656	122.060	b
M=5.9								
Livermore	San Ramon	(cdmg 0134)	70	340	22.5	37.780	121.980	c
Jan. 27, 1980	APEEL 3E	(cdmg 0219)	236	146	37.8	37.656	122.060	b
M=5.2	Morgan Territory Pk, Livermore	(cdmg 0000)	355	265	10.1	37.818	121.795	b
Westmoreland	Brawley Airport	(usgs 5060)	135	225	11.2	32.990	115.510	c
Apr 26, 1981	Parachute Test Site	(usgs 5247)	315	225	2.6	32.930	115.700	b
M=5.6	Salton Sea Wildlife Refuge	(usgs 5062)	315	225	0.6	33.180	115.620	c
	Superstition Mtn	(usgs 286)	135	45	9.2	32.950	115.820	b
	Westmoreland	(cdmg 11369)	90	180	0.5	33.037	115.623	c
Morgan Hill	Anderson Dam (downstream)	(usgs 1652)	340	250	3.8	37.165	121.631	b
April 24, 1984	Gilroy #1	(cdmg 47379)	67	337	17.6	36.973	121.572	a
M=6.2	Gilroy #2	(cdmg 47380)	90	0	16.6	36.982	121.556	c
	Gilroy #4	(cdmg 57382)	360	270	14.5	37.005	121.522	c
	Gilroy #6	(cdmg 57383)	90	0	13.6	37.026	121.484	b
	Gilroy #7	(cdmg 57425)	0	–	15.8	37.033	121.434	c
	Halls Valley	(cdmg 57191)	240	150	0.3	37.338	121.714	c
	Hollister Airport diff. array	(usgs 1656)	255	165	30.1	36.888	121.413	c
	Gilroy #3	(cdmg 47381)	90	0	16.2	36.987	121.536	c
	Gilroy, Gavilan College	(cdmg 47006)	67	23	17.6	36.973	121.568	b

Whittier	Alhambra-Fremont sch.	(cdmg 24461)	270	180	3.8	34.070	118.150	b
Oct. 1, 1987	LA Country Club North	(cdmg 24389)	90	0	28.5	34.063	118.418	c
M=6.0	LA Country Club South	(cdmg 24390)	90	0	28.3	34.062	118.416	c
	LA Hollywd Storage bld. ff	(cdmg 24303)	90	0	21.2	34.090	118.339	c
	Lake Hughes #1	(cdmg 24271)	90	0	72.3	34.674	118.430	b
	Rancho Cucamonga - L&J	(cdmg 23497)	90	0	43.2	34.104	117.574	b
	Sylmar	(cdmg 24514)	90	0	41.5	34.326	118.444	c
	Tarzana	(cdmg 24436)	90	0	40.3	34.160	118.534	b
	17645 Saticoy St., Northridge	(usc 03)	180	90	40.4	34.209	118.517	c
	13232 Kagel Can. Rd, Pacoima	(usc 05)	45	315	34.6	34.251	118.420	b
	9210 Sunland Bvd., Sun Valley	(usc 08)	310	220	29.6	34.235	118.367	b
	Coldwater Cany. ., Studio City	(usc 10)	182	92	29.1	34.146	118.413	c
	542 N. Buena vista St., Burbank	(usc 12)	340	250	23.0	34.168	118.332	c
	Mulholland Dr., Beverly Hills	(usc 13)	9	279	31.1	34.132	118.439	c
	Mulholland Dr., Beverly HIlls	(usc 14)	122	32	27.9	34.127	118.405	b
	700 N. Faring Rd., LA	(usc 16)	90	0	30.1	34.089	118.435	b
	600 E. Grand Ave., San Gabriel	(usc 19)	270	180	0.8	34.091	118.093	b
	4312 S. Grand Ave., LA	(usc 22)	180	90	16.7	34.005	118.279	c
	2369 E. Vernon Ave., LA	(usc 25)	173	83	12.6	34.004	118.230	c
	5921 N. Figueroa St., LA	(usc 32)	58	328	8.4	34.111	118.189	b
	624 Cypress Ave., LA	(usc 33)	143	53	10.5	34.088	118.222	b
	3035 Fletcher Dr., LA	(usc 34)	234	144	13.2	34.115	118.244	c
	Sunset Blvd., Pacific Palisades	(usc 49)	280	190	41.1	34.042	118.554	c
	Pacific Coast Hyw., Malibu	(usc 51)	150	60	62.7	34.024	118.787	b
	Las Virgines Rd., Calabasas	(usc 52)	290	200	54.8	34.151	118.696	b
	Lst. Can. Rd., Canyon Country	(usc 57)	0	270	48.0	34.419	118.426	c
	New York Ave., La Crescenta	(usc 60)	180	90	22.4	34.238	118.253	c
	Big Tujunga Station	(usc 61)	352	262	25.4	34.286	118.225	b
	Angeles Nat. For., Mill Creek	(usc 62)	90	0	33.9	34.390	118.079	c
	Las Palmas Ave., Glendale	(usc 63)	267	177	17.8	34.200	118.231	b
	120 N. Oakbank, Glendora	(usc 65)	170	80	16.2	34.137	117.882	b
	656 S. Grand Ave., Covina	(usc 68)	105	15	15.8	34.078	117.870	c
	Holly Ave., Baldwin Park	(usc 69)	270	180	6.7	34.100	117.974	b
	1271 W. Badillo, Covina	(usc 70)	0	270	11.7	34.087	117.915	c
	1307 S. Orange, West Covina	(usc 71)	315	225	8.2	34.064	117.952	c
	504 Rimgrove Ave., La Puente	(usc 72)	105	15	11.8	34.026	117.918	c
	Colima Rd., Hacienda Heights	(usc 73)	230	140	11.0	33.990	117.942	c
	950 Briarcliff Dr., La Habra	(usc 74)	90	0	13.5	33.921	117.972	c
	E. Joslin St., Sante Fe Springs	(usc 77)	48	318	8.6	33.944	118.087	c
	Castlegate St., Compton	(uscs78)	0	270	16.5	33.899	118.196	c
	12500 Birchdale, Downey	(usc 79)	180	90	11.9	33.920	118.137	c
	6979 Orange Ave., Long Beach	(usc 80)	10	280	17.3	33.881	118.176	c
	21288 Water St., Carson	(usc 81)	270	180	24.5	33.836	118.239	c
	6701 Del Amo, Lakewood	(usc 84)	90	0	19.4	33.846	118.099	c
	5360 Saturn St., LA	(usc 91)	110	20	22.7	34.046	118.355	c
	180 Campus Dr., Arcadia	(usc 93)	9	279	5.4	34.130	118.036	b
	7420 Jaboneria, Bell Gardens	(usc 94)	297	207	8.5	33.965	118.158	c
	1488 Old House Rd., Pasadena	(usc 95)	90	0	9.7	34.171	118.079	c
Loma Prieta	Anderson Dam: Downstream	(usgs 1652)	340	250	20.0	37.166	121.628	b
Oct. 18, 1989	Hollister Airport Diff Array	(usgs 1656)	255	165	25.4	36.888	121.413	c
M=6.9	Hollister City Hall Annex	(usgs 1575)	180	90	27.8	36.851	121.402	c
	Stanford SLAC Test lab	(usgs 1601)	360	270	35.0	37.419	122.205	c
	Hayward City Hall N. FF	(usgs 1129)	64	334	58.7	37.679	122.082	b

	APEEL station 9	(usgs 1161)	227	137	46.4	37.478	122.321	b
	Bear Valley sta. 5	(usgs 1474)	310	220	53.7	36.673	121.195	b
	Bear Valley sta. 10	(usgs 1479)	310	220	67.3	36.532	121.143	c
	Bear Valley sta. 12	(usgs 1481)	310	220	50.9	36.658	121.249	c
	Calaveras Res. South gnd.	(usgs 1687)	180	90	36.1	37.452	121.807	b
	Cherry Flat Reservoir	(usgs 1696)	360	270	32.5	37.396	121.756	a
	Dublin Fire Station	(usgs 1689)	360	270	61.6	37.709	121.932	c
	Hollister Sago Vault	(usgs 1032)	360	270	29.9	36.765	121.446	a
	Sunol Fire Station	(usgs 1688)	180	90	49.9	37.597	121.880	b
	Agnew	(cdmg 57066)	90	0	27.0	37.397	121.952	c
	Gilroy # 1	(cdmg 47379)	90	0	10.5	36.973	121.572	a
	Monterey city hall	(cdmg 47377)	90	0	42.7	36.597	121.897	a
	San Fran. Sierra Point	(cdmg 58539)	205	115	67.6	37.674	122.388	a
	Corralitos	(cdmg 57007)	90	0	0.1	37.046	121.803	b
	Gilroy #1 Gavilan College	(cdmg 47006)	67	337	10.9	36.973	121.568	b
	Saratoga	(cdmg 58065)	90	0	11.7	37.255	122.031	b
	Santa Cruz	(cdmg 58135)	90	0	12.5	37.001	122.060	b
	San Jose: Santa Teresa Hills	(cdmg 57563)	225	315	13.2	37.210	121.803	b
	Gilroy #6	(cdmg 57383)	90	0	19.9	37.026	121.484	b
	SAGO south	(cdmg 47189)	351	261	34.1	36.753	121.396	b
	Woodside	(cdmg 58127)	90	0	38.7	37.429	122.258	b
	Hayward BART FF	(cdmg 58498)	310	220	57.7	37.670	122.086	b
	Capitola	(cdmg 47125)	90	0	8.6	36.974	121.952	c
	Gilroy #2	(cdmg 47380)	90	0	12.1	36.982	121.556	c
	Gilroy #3	(cdmg 47381)	90	0	14.0	36.987	121.536	c
	Gilroy #4	(cdmg 57382)	90	0	15.8	37.005	121.522	c
	Gilroy #7	(cdmg 57425)	90	0	24.3	37.033	121.434	c
	Halls Valley	(cdmg 57191)	90	0	29.3	37.338	121.714	c
	Salinas	(cdmg 47179)	250	160	31.4	36.671	121.642	c
	Fremont	(cdmg 57064)	90	0	42.4	37.535	121.929	c
	San Fran. Airport	(cdmg 58223)	90	0	63.2	37.622	122.398	c
Sierra Madre	17645 Saticoy St., Northridge	(usc 03)	180	90	44.0	34.209	118.517	c
June 28, 1991	600 E. Grand Ave., San Gabriel	(usc 19)	270	180	17.7	34.091	118.093	b
M=5.6	3035 Fletcher Dr., LA	(usc 34)	234	144	23.8	34.115	118.244	c
	Canoga Park	(usc 53)	196	106	52.1	34.212	118.606	c
	Lst. Can. Rd., Canyon Country	(usc 57)	0	270	39.9	34.419	118.426	c
	New York Ave., La Crescenta	(usc 60)	180	90	19.6	34.238	118.254	c
	Big Tujunga Station	(usc 61)	352	262	17.3	34.286	118.225	b
	Las Palmas Ave., Glendale	(usc 63)	267	177	18.4	34.200	118.231	b
	120 N. Oakbank, Glendora	(usc 65)	170	80	14.8	34.137	117.883	b
	11338 Fariview Ave., El Monte	(usc 66)	185	95	16.7	34.093	118.019	c
	237 Mel Canyon Rd., Duarte	(usc 67)	180	90	11.6	34.150	117.939	b
	Holly Ave., Baldwin Park	(usc 69)	270	180	16.1	34.100	117.974	b
	1271 W. Badillo, Covina	(usc 70)	0	270	18.9	34.087	117.915	c
	1307 S. Orange, West Covina	(usc 71)	315	225	20.4	34.064	117.952	c
	E. Joslin St., Sante Fe Springs	(usc 77)	48	318	33.5	33.944	118.087	c
	180 Campus Dr., Arcadia	(usc 93)	9	279	12.6	34.130	118.036	b
	7420 Jaboneria, Bell Gardens	(usc 94)	310	220	32.8	33.965	118.158	c
	855 Arcadia Ave., Arcadia	(usc 99)	262	172	13.1	34.127	118.059	c
Petrolia	Ferndale Fire Sta	(usgs 1023)	360	270	10.0	40.576	124.262	c
April 25, 1992	Loleta Fire Sta	(usgs 1586)	360	270	17.6	40.644	124.219	b
M=7.1	Centerville Beach	(usgs 1585)	360	270	9.8	40.563	124.348	b
	College of Redwood	(usgs 1582)	360	270	23.9	40.699	124.200	b

	South Bay school	(usgs 1581)	360	270	27.8	40.735	124.207	c
	Fortuna Fire Sta	(usgs 1583)	360	270	14.6	40.599	124.154	b
	Bunker Hill FAA	(usgs 1584)	360	270	1.9	40.498	124.294	a
Landers	Twentynine Palms	(cdmg 22161)	90	0	41.9	34.021	116.009	a
June 28, 1992	Silent Valley	(cdmg 12206)	90	0	51.3	33.851	116.852	a
M=7.3	Joshua Tree	(cdmg 22170)	90	0	11.3	34.131	116.314	b
	Desert hot Springs	(cdmg 12149)	90	0	22.5	33.962	116.509	b
	Barstow	(cdmg 23559)	90	0	37.7	34.887	117.047	b
	Fort irwin	(cdmg 24577)	90	0	65.0	35.268	116.684	b
	Yermo	(cdmg 22074)	90	0	26.3	34.903	116.823	c
	Palm Springs	(cdmg 12025)	90	0	36.7	33.829	116.501	c
	Indio	(cdmg 12026)	90	0	54.9	33.717	116.156	c
	Amboy	(cdmg 21081)	90	0	68.3	34.560	115.743	a
	Baker	(cdmg 32075)	140	50	88.3	35.272	116.066	b
	Boron	(cdmg 33083)	90	0	92.4	35.002	117.650	b
	Hemet	(cdmg 12331)	90	0	69.1	33.729	116.979	c
	Puerta La Cruz	(cdmg 12168)	90	0	95.0	33.324	116.683	b
	Riverside Airport	(cdmg 13123)	270	180	96.2	33.951	117.446	b
	San Bernadino E & H	(cdmg 23542)	90	180	79.9	34.065	117.292	c
	N. Palm Sprngs fs	(usgs 5295)	180	90	27.7	33.924	116.543	b
	Whitewater Canyon	(usgs 5072)	270	180	27.6	33.989	116.655	a
	Morongo Valley	(usgs 5071)	135	45	17.7	34.048	116.577	b
	Forest Falls	(usgs 5075)	300	210	45.4	34.088	116.919	b
	Indio Jackson rd	(usgs 5294)	180	90	49.6	33.747	116.214	c
	Fun Valley	(usgs 5069)	135	45	25.8	33.930	116.390	b
	Thousand Palms	(usgs 5068)	135	45	37.7	33.820	116.400	c
	Euclid st., Fountain Valley	(usc 02)	22	292	144.2	33.719	117.938	c
	Roscoe Blvd., Sun Valley	(usc 06)	90	0	162.8	34.221	118.421	b
	Buena Vista St., Burbank	(usc 12)	340	250	157.2	34.168	118.332	c
	924 W. 70th St., LA	(usc 23)	0	270	163.0	33.976	118.289	c
	5921 N. Figueroa St., LA	(usc 32)	58	328	147.8	34.111	118.189	b
	3036 Fletcher Dr., LA	(usc 34)	234	144	152.2	34.115	118.244	c
	N. Las Virginies Rd., Calabasas	(usc 52)	290	200	189.4	34.151	118.697	b
	Mt. Gleason Ave., Sunland	(usc 58)	260	170	150.8	34.269	118.303	b
	Big Tujunga Station	(usc 61)	352	262	143.4	34.286	118.225	b
	Las Palmas Ave., Glendale	(usc 63)	267	177	147.3	34.200	118.231	c
	120 N. Oakbank, Glendora	(usc 65)	170	80	121.5	34.137	117.882	b
	Colima Rd., Hacienda Heights	(usc 73)	230	140	135.1	33.990	117.942	c
	180 Campus Dr., Arcadia	(usc 93)	9	279	134.3	34.130	118.036	b
Big Bear	Big Bear Lake - civic center	(cdmg 22561)	270	360	10.2	34.238	116.935	b
June 28, 1992	San Bernadino E & H	(cdmg 23542)	90	180	39.7	34.065	117.292	c
M=6.2	N.Palm Springs FS	(usgs 5295)	180	90	36.2	33.924	116.543	b
	San Bernadino, Highland FS	(usgs 5161)	315	225	31.3	34.136	117.213	c
	Morongo Valley	(usgs 5071)	135	45	24.6	34.048	116.577	b
	Fun Valley	(usgs 5069)	135	45	45.7	33.930	116.390	b
	Euclid st., Fountain Valley	(usc 02)	22	292	109.2	33.719	117.938	c
	120 N. Oakbank, Glendora	(usc 65)	170	80	93.0	34.137	117.882	b
	656 S. Grand Ave., Covina	(usc 68)	74	344	92.4	34.078	117.871	c
	1271 W. Badillo, Covina	(usc 70)	0	270	96.3	34.087	117.915	c
	504 Rimgrove Ave., La Puente	(usc 72)	105	15	97.4	34.026	117.918	c
	Colima Rd., Hacienda Heights	(usc 73)	230	140	100.2	33.990	117.942	c
	E. Joslin St., Santa Fe Springs	(usc 77)	120	30	114.3	33.944	118.087	c
	200 S. Flower Ave., Brea	(usc 87)	20	290	97.9	33.916	117.896	c

	17852 Serrano Ave., Villa Park	(usc 90)	0	270	94.4	33.821	117.818	b
	180 Campus Dr., Arcadia	(usc 93)	9	279	107.2	34.130	118.036	b
	7420 Jaboneria, Bell Gardens	(usc 94)	310	220	120.3	33.965	118.158	c
Northridge	Alhambra - Fremont Sch.	(cdmg 24461)	90	360	36.2	34.070	118.150	b
Jan. 17, 1994	Castaic Old Ridge Rt.	(cdmg 24278)	90	360	20.8	34.564	118.642	b
M=6.7	Century City - LACC north	(cdmg 24389)	90	360	17.4	34.063	118.418	c
	Lake Hughes #1 fs	(cdmg 24271)	90	0	36.1	34.674	118.430	b
	Lake Hughes 4	(cdmg 24469)	90	0	31.9	34.650	118.478	c
	Lake Hughes #4b	(cdmg 24523)	90	0	32.0	34.650	118.477	c
	Lake Hughes #9	(cdmg 24272)	90	360	25.6	34.608	118.558	a
	Lake Hughes #12a	(cdmg 24607)	90	180	21.5	34.571	118.560	b
	Littlerock - Brainard Canyon	(cdmg 23595)	90	180	46.7	34.486	117.980	a
	Long Beach - City Hall grounds	(cdmg 14560)	90	360	56.0	33.768	118.196	c
	LA - Hollywood stor.blg.	(cdmg 24303)	90	360	20.0	34.090	118.339	c
	Mt. Baldy - Elem. School	(cdmg 23572)	90	180	72.2	34.233	117.661	a
	Mt. Wilson	(cdmg 24399)	90	360	36.5	34.224	118.057	a
	Phelan - Wilson Ranch Rd.	(cdmg 23597)	90	180	86.4	34.467	117.520	b
	Port Hueneme - Naval Lab.	(cdmg 25281)	180	90	49.8	34.145	119.206	c
	Rancho Cucamonga-Deer Can.	(cdmg 23598)	90	180	80.8	34.169	117.579	a
	Rancho Cucamonga - L&J FF	(cdmg 23497)	90	0	82.9	34.104	117.574	b
	Rancho Palos Verdes	(cdmg 14404)	90	0	50.8	33.746	118.396	a
	Riverside airport	(cdmg 13123)	270	180	99.8	33.951	117.446	b
	San Bernardino - E & H	(cdmg 23542)	90	180	109.2	34.065	117.292	c
	Sylmar - County Hospital PL	(cdmg 24514)	90	360	1.7	34.326	118.444	c
	Tarzana Cedar Hill Nur. A	(cdmg 24436)	90	360	3.4	34.160	118.534	b
	Wrightwood - Jackson Flat	(cdmg 23590)	90	180	65.2	34.381	117.737	a
	Wrightwood - Nielson Ranch	(cdmg 23573)	90	180	82.4	34.314	117.545	b
	Wrightwood - Swarthout Valley	(cdmg 23574)	90	180	72.3	34.369	117.658	b
	17645 Saticoy St. Northridge	(usc 03)	180	90	0.2	34.209	118.517	c
	12001 Chalon Rd. LA	(usc 15)	70	160	12.4	34.086	118.481	b
	700 N. Faring Rd, LA	(usc 16)	0	90	14.1	34.089	118.435	b
	8510 Wonderland Ave, LA	(usc 17)	185	95	15.4	34.114	118.380	a
	Willoughby Ave. Hollywood	(usc 18)	180	90	18.3	34.088	118.365	b
	600 E. Grand Av., San Gabriel	(usc 19)	180	270	39.4	34.091	118.093	b
	2628 W. 15th. St., LA	(usc 20)	180	90	26.1	34.045	118.298	c
	4312 S. Grand Ave, LA	(usc 22)	180	90	30.4	34.005	118.279	c
	2369 E. Vernon Ave, LA	(usc 25)	180	90	33.8	34.004	118.230	c
	624 Cypress Ave., LA	(usc 33)	53	143	29.4	34.088	118.222	b
	3036 Fletcher Dr., LA	(usc 34)	144	234	26.2	34.115	118.244	c
	23536 Catskill Ave., Carson	(usc 40)	180	90	48.3	33.812	118.270	c
	Rancho Palos Verdes	(usc 44)	5	95	53.1	33.740	118.335	c
	14801 Osage Ave, Lawndale	(usc 45)	182	92	36.7	33.897	118.346	c
	Manhattan Beach	(usc 46)	0	90	36.1	33.886	118.389	c
	Canoga Park	(usc 53)	196	106	1.6	34.212	118.606	c
	3960 Centinela St., LA	(usc 54)	155	245	22.9	34.001	118.431	c
	Canyon Country	(usc 57)	0	270	11.4	34.419	118.426	c
	1250 Howard rd., Burbank	(usc 59)	330	60	16.5	34.204	118.302	a
	New York Ave., La Crescenta	(usc 60)	180	90	18.8	34.238	118.254	c
	Big Tujunga Station	(usc 61)	352	262	19.9	34.286	118.225	b
	3320 Las Palmas Ave., Glendale	(usc 63)	177	267	22.3	34.200	118.231	b
	120 N. Oakbank, Glendora	(usc 65)	80	170	54.8	34.137	117.882	b
	Fairview Ave., El Monte	(usc 66)	185	95	45.2	34.093	118.019	c
	237 Mel Canyon Rd., Duarte	(usc 67)	90	180	49.3	34.150	117.939	b
	656 S. Grand Ave., Covina	(usc 68)	344	74	58.1	34.078	117.871	c

3699 Holly Ave., Baldwin Park	(usc 69)	180	270	48.5	34.100	117.974	b
1271 W. Badillo, Covina	(usc 70)	360	270	54.0	34.087	117.915	c
S. Orange Ave., West Covina	(usc 71)	315	225	52.1	34.064	117.952	c
504 Rimgrove Ave., La Puente	(usc 72)	15	105	57.0	34.026	117.918	c
Colima Rd., Hacienda Heights	(usc 73)	140	230	57.3	33.990	117.942	c
6302 S. Alta Dr. Whittier	(usc 75)	0	90	48.9	34.015	118.029	b
E. Joslin St., Santa Fe Springs	(usc 77)	30	120	48.3	33.944	118.087	c
14637 Castlegate st., Compton	(usc 78)	360	270	44.2	33.899	118.196	c
21288 Water St., Carson	(usc 81)	180	270	47.4	33.836	118.240	c
Terminal Island	(usc 82)	330	240	55.8	33.736	118.269	c
Huntington Beach	(usc 83)	290	200	67.9	33.727	118.044	c
Del Amo Blvd., Lakewood	(usc 84)	0	90	54.6	33.846	118.099	c
6861 Santa Rita, Garden Grove	(usc 85)	360	270	64.7	33.790	118.012	c
La Palma ave., Buena Park	(usc 86)	180	90	60.0	33.847	118.018	c
200 S. Flower Ave., Brea	(usc 87)	20	290	64.9	33.916	117.896	c
2000 W. Ball Rd., Anaheim	(usc 88)	0	90	66.9	33.817	117.951	c
5360 Saturn St., LA	(usc 91)	20	110	22.3	34.046	118.355	c
180 Campus Dr., Arcadia	(usc 93)	9	279	41.9	34.130	118.036	b
7420 Jaboneria, Bell Gardens	(usc 94)	310	220	41.7	33.965	118.158	c
3620 S. Vermont Ave., LA	(usc 96)	0	90	28.1	34.022	118.293	c
855 Arcadia Ave., Arcadia	(usc 99)	172	262	40.1	34.127	118.059	c
Griffith Observatory	(usgs 141)	360	270	21.5	34.118	118.299	a
Littlerock Post Office	(usgs 5030)	300	210	47.6	34.520	117.990	b
Pardo Dam Downstream	(usgs 969)	90	360	86.7	33.890	117.641	c
Long Beach VA Hospital	(usgs 5106)	360	270	59.2	33.778	118.118	b
NSMP Pasadena Lab.	(usgs 5296)	360	270	34.1	34.136	118.127	b

* ct: California Institute of Technology Civil Engineering Dept.
usc: University of Southern California Civil Engineering Dept.
cdmg: California Division of Mines and Geology Strong Motion Instrumentation Program
usgs: U. S. Geological Survey National Strong Motion Program

Table 3.2

NEHRP* Site Class

Site Class	Range of Shear Velocities
A	>1500 m/s
B	760 m/s to 1500 m/s
C	360 m/s to 760 m/s
D	180 m/s to 360 m/s
E	< 180 m/s

* BSSC (1994)

Table 3.3

Regression Coefficients for Peak Ground Acceleration and Velocity, Randomly Oriented Horizontal Component

PGA

a	b	c	d	h	e	f	σ
3.098	0.3065	-0.07570	-0.8795	6.910	0.1452	0.1893	0.2124

PGV

a	b	c	d	h	e	f	σ
1.747	0.4481	-0.03248	-0.8075	3.992	0.1862	0.3009	0.2470

Regression coefficients refer to Equation 3.7, for the base 10 logarithm of motion, PGA in units of cm/sec^2 and PGV in units of cm/sec.

TABLE 3.4

PSV 2% Damping

Regression coefficients refer to Equation 3.7, for the base 10 logarithm of motion, randomly oriented horizontal component (cm/sec)

Freq. (Hz)	a	b	c	d	h	e	f	σ
0.500	1.581	0.638	-0.037	-0.695	2.773	0.267	0.452	0.326
0.526	1.588	0.631	-0.061	-0.693	3.123	0.293	0.474	0.327
0.556	1.614	0.627	-0.070	-0.694	3.427	0.296	0.471	0.326
0.588	1.637	0.607	-0.060	-0.693	3.512	0.290	0.468	0.319
0.625	1.700	0.599	-0.059	-0.731	3.664	0.291	0.472	0.311
0.667	1.715	0.586	-0.033	-0.748	3.476	0.303	0.476	0.302
0.714	1.709	0.569	-0.039	-0.717	2.966	0.282	0.450	0.302
0.769	1.745	0.541	-0.047	-0.708	2.945	0.260	0.429	0.306
0.833	1.814	0.544	-0.070	-0.703	3.340	0.216	0.388	0.290
0.909	1.774	0.524	-0.079	-0.658	3.163	0.213	0.391	0.288
1.000	1.844	0.501	-0.045	-0.700	3.723	0.219	0.372	0.277
1.053	1.871	0.496	-0.039	-0.724	3.383	0.223	0.368	0.282
1.111	1.891	0.500	-0.043	-0.738	3.201	0.218	0.368	0.287
1.176	1.875	0.497	-0.047	-0.733	2.881	0.226	0.376	0.284
1.250	1.866	0.493	-0.060	-0.716	2.674	0.202	0.361	0.290
1.333	1.915	0.494	-0.074	-0.753	2.850	0.224	0.368	0.292
1.429	1.974	0.505	-0.082	-0.796	3.304	0.221	0.375	0.294
1.538	2.013	0.463	-0.057	-0.798	3.472	0.183	0.343	0.291
1.667	2.023	0.465	-0.087	-0.795	3.717	0.197	0.335	0.292
1.818	1.973	0.406	-0.065	-0.741	3.512	0.195	0.340	0.279
2.000	2.001	0.390	-0.057	-0.768	4.388	0.224	0.352	0.269
2.083	1.985	0.380	-0.053	-0.757	4.137	0.219	0.343	0.271
2.174	1.958	0.364	-0.051	-0.733	3.963	0.213	0.337	0.274
2.273	1.986	0.368	-0.053	-0.742	3.952	0.188	0.307	0.278
2.381	2.023	0.367	-0.069	-0.761	4.186	0.187	0.287	0.274
2.500	2.045	0.333	-0.043	-0.777	4.538	0.177	0.283	0.268
2.632	2.099	0.321	-0.043	-0.804	5.036	0.158	0.256	0.262
2.778	2.096	0.338	-0.063	-0.814	5.274	0.182	0.266	0.266
2.941	2.122	0.341	-0.080	-0.814	5.361	0.165	0.235	0.262
3.125	2.101	0.349	-0.090	-0.809	5.413	0.166	0.235	0.262
3.333	2.083	0.358	-0.116	-0.796	5.859	0.171	0.237	0.255
3.571	2.204	0.370	-0.131	-0.867	7.914	0.153	0.198	0.246
3.846	2.160	0.359	-0.123	-0.858	8.085	0.154	0.186	0.243
4.167	2.219	0.362	-0.121	-0.906	8.782	0.143	0.170	0.243
4.545	2.193	0.350	-0.129	-0.895	9.549	0.151	0.165	0.238
5.000	2.325	0.370	-0.163	-0.962	11.380	0.117	0.116	0.238
5.263	2.271	0.363	-0.166	-0.953	10.400	0.125	0.130	0.238
5.556	2.275	0.335	-0.155	-0.975	10.590	0.132	0.130	0.241
5.882	2.200	0.318	-0.156	-0.953	10.870	0.155	0.145	0.243
6.250	2.313	0.303	-0.140	-1.029	12.470	0.130	0.126	0.241
6.667	2.314	0.310	-0.150	-1.052	12.850	0.123	0.121	0.239
7.143	2.325	0.301	-0.134	-1.111	12.850	0.147	0.139	0.243
7.692	2.265	0.299	-0.124	-1.098	12.920	0.124	0.117	0.240
8.333	2.185	0.308	-0.128	-1.085	11.860	0.098	0.101	0.234
9.091	2.096	0.252	-0.079	-1.092	11.400	0.112	0.113	0.252
10.00	2.061	0.254	-0.090	-1.096	11.570	0.091	0.087	0.247

TABLE 3.5

PSV 5% Damping

Regression coefficients refer to Equation 3.7, for the base 10 logarithm of motion, randomly oriented horizontal component (cm/sec)

Freq. (Hz)	a	b	c	d	h	e	f	σ
0.500	1.547	0.627	-0.046	-0.729	2.929	0.275	0.449	0.316
0.526	1.563	0.621	-0.066	-0.724	3.145	0.279	0.451	0.318
0.556	1.572	0.609	-0.065	-0.722	3.302	0.287	0.456	0.315
0.588	1.593	0.597	-0.065	-0.722	3.400	0.288	0.459	0.310
0.625	1.634	0.588	-0.063	-0.744	3.543	0.294	0.464	0.304
0.667	1.648	0.575	-0.048	-0.755	3.390	0.300	0.463	0.299
0.714	1.654	0.554	-0.046	-0.733	3.005	0.276	0.433	0.297
0.769	1.713	0.542	-0.055	-0.739	3.121	0.243	0.404	0.297
0.833	1.767	0.530	-0.061	-0.739	3.401	0.211	0.380	0.285
0.909	1.750	0.516	-0.074	-0.706	3.302	0.204	0.374	0.283
1.000	1.789	0.490	-0.047	-0.730	3.561	0.216	0.368	0.277
1.053	1.822	0.489	-0.043	-0.753	3.420	0.213	0.360	0.279
1.111	1.834	0.487	-0.043	-0.765	3.182	0.211	0.361	0.283
1.176	1.830	0.486	-0.045	-0.771	2.983	0.222	0.371	0.284
1.250	1.830	0.481	-0.054	-0.768	2.914	0.217	0.368	0.285
1.333	1.869	0.480	-0.062	-0.796	3.087	0.225	0.370	0.287
1.429	1.904	0.482	-0.072	-0.812	3.367	0.214	0.363	0.292
1.538	1.939	0.454	-0.052	-0.823	3.503	0.189	0.344	0.288
1.667	1.930	0.442	-0.072	-0.810	3.562	0.200	0.341	0.286
1.818	1.923	0.406	-0.061	-0.792	3.850	0.204	0.342	0.277
2.000	1.914	0.376	-0.049	-0.787	4.116	0.217	0.350	0.270
2.083	1.898	0.362	-0.046	-0.774	3.955	0.214	0.344	0.271
2.174	1.885	0.350	-0.042	-0.759	3.942	0.204	0.332	0.271
2.273	1.894	0.344	-0.041	-0.761	3.999	0.191	0.315	0.272
2.381	1.929	0.344	-0.051	-0.779	4.208	0.181	0.296	0.270
2.500	1.964	0.329	-0.048	-0.799	4.545	0.173	0.283	0.264
2.632	1.972	0.315	-0.048	-0.807	4.767	0.171	0.278	0.262
2.778	1.981	0.324	-0.059	-0.818	4.948	0.179	0.274	0.264
2.941	1.998	0.322	-0.066	-0.826	5.236	0.178	0.262	0.260
3.125	1.997	0.335	-0.085	-0.824	5.409	0.177	0.249	0.256
3.333	1.998	0.340	-0.105	-0.824	5.854	0.177	0.240	0.248
3.571	2.060	0.344	-0.111	-0.865	7.022	0.164	0.211	0.242
3.846	2.082	0.346	-0.114	-0.885	7.589	0.156	0.187	0.237
4.167	2.090	0.347	-0.115	-0.906	8.303	0.157	0.188	0.236
4.545	2.101	0.341	-0.127	-0.915	9.229	0.152	0.175	0.232
5.000	2.181	0.350	-0.149	-0.962	10.670	0.132	0.138	0.230
5.263	2.153	0.345	-0.151	-0.964	10.270	0.139	0.144	0.229
5.556	2.146	0.334	-0.150	-0.976	10.260	0.139	0.143	0.230
5.882	2.102	0.319	-0.151	-0.967	10.450	0.148	0.149	0.232
6.250	2.115	0.301	-0.133	-0.990	10.790	0.136	0.137	0.229
6.667	2.108	0.300	-0.133	-1.010	11.050	0.130	0.130	0.230
7.143	2.121	0.297	-0.126	-1.053	11.670	0.141	0.146	0.228
7.692	2.057	0.285	-0.109	-1.047	11.570	0.138	0.144	0.225
8.333	1.986	0.284	-0.106	-1.033	10.850	0.114	0.123	0.224
9.091	1.915	0.254	-0.075	-1.044	10.540	0.120	0.135	0.233
10.000	1.857	0.248	-0.071	-1.044	10.430	0.112	0.121	0.230

TABLE 3.6

PSV 10% Damping

Regression coefficients refer to Equation 3.7, for the base 10 logarithm of motion, randomly oriented horizontal component (cm/sec)

Freq. (Hz)	a	b	c	d	h	e	f	σ
0.500	1.488	0.612	-0.053	-0.739	3.006	0.271	0.439	0.309
0.526	1.509	0.605	-0.062	-0.742	3.142	0.276	0.440	0.308
0.556	1.526	0.601	-0.067	-0.743	3.227	0.277	0.439	0.307
0.588	1.546	0.590	-0.067	-0.746	3.324	0.280	0.441	0.303
0.625	1.569	0.581	-0.065	-0.756	3.389	0.284	0.447	0.300
0.667	1.581	0.564	-0.056	-0.757	3.346	0.285	0.444	0.297
0.714	1.602	0.544	-0.051	-0.754	3.173	0.269	0.425	0.295
0.769	1.653	0.534	-0.053	-0.757	3.233	0.237	0.396	0.291
0.833	1.698	0.524	-0.058	-0.759	3.391	0.211	0.375	0.285
0.909	1.703	0.506	-0.054	-0.747	3.370	0.201	0.368	0.283
1.000	1.719	0.484	-0.042	-0.753	3.433	0.209	0.365	0.279
1.053	1.739	0.479	-0.041	-0.765	3.381	0.208	0.361	0.280
1.111	1.759	0.473	-0.039	-0.781	3.259	0.212	0.363	0.281
1.176	1.768	0.471	-0.043	-0.791	3.134	0.215	0.366	0.281
1.250	1.773	0.472	-0.054	-0.797	3.134	0.221	0.370	0.282
1.333	1.797	0.470	-0.059	-0.811	3.261	0.221	0.366	0.284
1.429	1.822	0.463	-0.059	-0.819	3.384	0.209	0.355	0.287
1.538	1.838	0.438	-0.045	-0.824	3.469	0.198	0.347	0.284
1.667	1.840	0.422	-0.051	-0.819	3.573	0.197	0.341	0.284
1.818	1.838	0.400	-0.056	-0.806	3.870	0.203	0.341	0.276
2.000	1.827	0.365	-0.044	-0.793	3.919	0.204	0.336	0.270
2.083	1.818	0.352	-0.041	-0.787	3.891	0.202	0.333	0.270
2.174	1.820	0.345	-0.040	-0.786	3.933	0.195	0.324	0.268
2.273	1.828	0.340	-0.041	-0.789	4.013	0.188	0.315	0.267
2.381	1.847	0.333	-0.042	-0.799	4.198	0.182	0.304	0.266
2.500	1.861	0.325	-0.043	-0.808	4.433	0.178	0.296	0.262
2.632	1.862	0.315	-0.043	-0.814	4.547	0.178	0.292	0.262
2.778	1.865	0.308	-0.045	-0.821	4.716	0.183	0.289	0.261
2.941	1.882	0.312	-0.060	-0.828	5.076	0.181	0.275	0.256
3.125	1.894	0.321	-0.075	-0.833	5.419	0.182	0.258	0.252
3.333	1.910	0.326	-0.088	-0.845	5.814	0.179	0.243	0.245
3.571	1.945	0.332	-0.094	-0.870	6.477	0.166	0.218	0.240
3.846	1.954	0.338	-0.105	-0.882	6.968	0.160	0.202	0.236
4.167	1.960	0.337	-0.110	-0.896	7.619	0.161	0.198	0.232
4.545	1.980	0.336	-0.122	-0.909	8.460	0.147	0.177	0.226
5.000	1.999	0.335	-0.133	-0.931	9.285	0.141	0.158	0.223
5.263	1.997	0.338	-0.140	-0.941	9.477	0.145	0.157	0.221
5.556	1.991	0.334	-0.143	-0.950	9.512	0.142	0.154	0.221
5.882	1.964	0.324	-0.141	-0.950	9.492	0.141	0.152	0.222
6.250	1.954	0.308	-0.129	-0.961	9.630	0.135	0.146	0.222
6.667	1.934	0.301	-0.123	-0.972	9.669	0.132	0.143	0.222
7.143	1.916	0.296	-0.117	-0.988	10.060	0.137	0.151	0.220
7.692	1.860	0.290	-0.108	-0.984	9.992	0.138	0.155	0.218
8.333	1.818	0.286	-0.102	-0.985	9.791	0.125	0.143	0.217
9.091	1.760	0.272	-0.086	-0.994	9.648	0.130	0.151	0.219
10.000	1.692	0.258	-0.071	-0.990	9.442	0.126	0.146	0.215

TABLE 3.7

V_{ea} 2% Damping

Regression coefficients refer to Equation 3.7, for the base 10 logarithm of motion, randomly oriented horizontal component (cm/sec)

Freq. (Hz)	a	b	c	d	h	e	f	σ
0.500	1.691	0.655	-0.046	-0.653	2.791	0.236	0.426	0.318
0.526	1.689	0.649	-0.066	-0.661	3.176	0.282	0.465	0.320
0.556	1.705	0.629	-0.060	-0.658	3.593	0.288	0.476	0.316
0.588	1.748	0.626	-0.071	-0.656	3.783	0.273	0.460	0.312
0.625	1.811	0.625	-0.064	-0.698	3.892	0.276	0.468	0.300
0.667	1.821	0.603	-0.027	-0.719	3.691	0.296	0.477	0.291
0.714	1.840	0.592	-0.032	-0.711	3.446	0.283	0.462	0.292
0.769	1.821	0.562	-0.044	-0.662	2.862	0.264	0.438	0.292
0.833	1.869	0.569	-0.079	-0.647	2.978	0.233	0.413	0.282
0.909	1.855	0.538	-0.069	-0.614	3.108	0.225	0.405	0.277
1.000	1.931	0.524	-0.043	-0.657	3.674	0.219	0.386	0.262
1.053	1.962	0.517	-0.040	-0.675	3.275	0.211	0.371	0.267
1.111	1.990	0.526	-0.051	-0.693	3.217	0.219	0.379	0.270
1.176	1.970	0.510	-0.044	-0.678	2.778	0.219	0.380	0.267
1.250	1.948	0.525	-0.072	-0.658	2.573	0.210	0.368	0.266
1.333	2.001	0.525	-0.069	-0.696	2.594	0.218	0.371	0.267
1.429	2.043	0.529	-0.080	-0.726	3.030	0.220	0.385	0.270
1.538	2.099	0.494	-0.059	-0.743	3.369	0.195	0.364	0.269
1.667	2.103	0.503	-0.089	-0.735	3.419	0.203	0.353	0.270
1.818	2.083	0.431	-0.050	-0.685	3.269	0.192	0.342	0.258
2.000	2.125	0.426	-0.047	-0.722	4.246	0.211	0.344	0.251
2.083	2.105	0.431	-0.055	-0.716	4.261	0.220	0.351	0.252
2.174	2.090	0.418	-0.053	-0.697	3.881	0.213	0.342	0.252
2.273	2.113	0.418	-0.064	-0.692	3.735	0.187	0.315	0.248
2.381	2.132	0.421	-0.074	-0.704	3.854	0.190	0.295	0.249
2.500	2.156	0.390	-0.042	-0.720	4.186	0.177	0.286	0.247
2.632	2.218	0.384	-0.041	-0.749	4.515	0.150	0.256	0.240
2.778	2.209	0.392	-0.066	-0.740	4.537	0.163	0.254	0.238
2.941	2.244	0.402	-0.074	-0.758	4.877	0.155	0.234	0.242
3.125	2.195	0.401	-0.084	-0.730	4.561	0.164	0.246	0.237
3.333	2.194	0.424	-0.102	-0.736	4.902	0.160	0.251	0.229
3.571	2.269	0.421	-0.102	-0.775	6.383	0.147	0.213	0.218
3.846	2.221	0.427	-0.107	-0.765	6.442	0.158	0.214	0.220
4.167	2.286	0.421	-0.086	-0.811	6.651	0.137	0.192	0.215
4.545	2.216	0.433	-0.099	-0.774	6.334	0.151	0.185	0.210
5.000	2.312	0.445	-0.118	-0.816	7.549	0.111	0.141	0.209
5.263	2.301	0.445	-0.128	-0.815	6.902	0.105	0.140	0.207
5.556	2.268	0.427	-0.113	-0.826	6.910	0.136	0.170	0.210
5.882	2.223	0.424	-0.114	-0.819	6.870	0.158	0.186	0.206
6.250	2.251	0.411	-0.098	-0.839	7.204	0.139	0.167	0.201
6.667	2.268	0.411	-0.097	-0.860	7.594	0.132	0.159	0.199
7.143	2.234	0.423	-0.102	-0.864	7.228	0.138	0.170	0.196
7.692	2.215	0.411	-0.068	-0.884	7.198	0.131	0.173	0.200
8.333	2.148	0.410	-0.061	-0.860	6.398	0.123	0.174	0.197
9.091	2.108	0.402	-0.040	-0.871	6.230	0.133	0.191	0.205
10.000	2.042	0.402	-0.042	-0.849	5.715	0.130	0.194	0.212

TABLE 3.8

V_{ea} 5% Damping

Regression coefficients refer to Equation 3.7, for the base 10 logarithm of motion, randomly oriented horizontal component (cm/sec)

Freq. (Hz)	a	b	c	d	h	e	f	σ
0.500	1.686	0.637	-0.050	-0.646	2.873	0.250	0.435	0.293
0.526	1.698	0.630	-0.059	-0.651	3.175	0.272	0.454	0.294
0.556	1.715	0.618	-0.062	-0.651	3.474	0.279	0.464	0.290
0.588	1.747	0.613	-0.068	-0.655	3.622	0.277	0.462	0.287
0.625	1.785	0.606	-0.057	-0.677	3.653	0.278	0.464	0.280
0.667	1.808	0.591	-0.039	-0.696	3.570	0.289	0.469	0.273
0.714	1.824	0.577	-0.041	-0.687	3.307	0.278	0.453	0.272
0.769	1.824	0.561	-0.055	-0.653	2.921	0.260	0.432	0.269
0.833	1.855	0.554	-0.073	-0.642	2.961	0.242	0.416	0.262
0.909	1.862	0.528	-0.061	-0.627	3.161	0.234	0.407	0.255
1.000	1.915	0.520	-0.050	-0.648	3.330	0.218	0.381	0.247
1.053	1.947	0.519	-0.050	-0.667	3.240	0.213	0.372	0.249
1.111	1.971	0.517	-0.050	-0.682	3.163	0.215	0.373	0.250
1.176	1.962	0.513	-0.053	-0.675	2.897	0.217	0.374	0.248
1.250	1.960	0.516	-0.064	-0.669	2.704	0.212	0.369	0.247
1.333	1.996	0.514	-0.065	-0.694	2.764	0.212	0.368	0.249
1.429	2.029	0.506	-0.066	-0.713	3.055	0.211	0.372	0.253
1.538	2.069	0.490	-0.065	-0.726	3.324	0.200	0.361	0.252
1.667	2.077	0.483	-0.078	-0.718	3.439	0.202	0.350	0.249
1.818	2.074	0.439	-0.054	-0.694	3.502	0.199	0.339	0.241
2.000	2.091	0.427	-0.050	-0.707	4.134	0.211	0.340	0.236
2.083	2.081	0.426	-0.055	-0.700	4.119	0.212	0.339	0.236
2.174	2.080	0.421	-0.058	-0.692	3.985	0.204	0.328	0.235
2.273	2.093	0.416	-0.063	-0.690	3.937	0.192	0.310	0.233
2.381	2.107	0.412	-0.065	-0.696	3.988	0.187	0.295	0.232
2.500	2.131	0.399	-0.056	-0.710	4.215	0.178	0.283	0.230
2.632	2.160	0.393	-0.056	-0.721	4.398	0.162	0.263	0.227
2.778	2.175	0.397	-0.068	-0.728	4.561	0.162	0.252	0.225
2.941	2.194	0.400	-0.077	-0.737	4.868	0.159	0.241	0.224
3.125	2.180	0.405	-0.087	-0.729	4.868	0.162	0.242	0.221
3.333	2.182	0.420	-0.099	-0.735	5.170	0.161	0.241	0.215
3.571	2.213	0.425	-0.106	-0.754	6.042	0.154	0.219	0.207
3.846	2.204	0.426	-0.105	-0.761	6.330	0.157	0.212	0.205
4.167	2.233	0.425	-0.095	-0.787	6.468	0.144	0.195	0.203
4.545	2.210	0.433	-0.102	-0.777	6.522	0.145	0.181	0.199
5.000	2.262	0.442	-0.117	-0.803	7.261	0.122	0.153	0.199
5.263	2.257	0.440	-0.121	-0.807	7.026	0.120	0.152	0.198
5.556	2.240	0.431	-0.115	-0.815	7.070	0.134	0.166	0.198
5.882	2.222	0.424	-0.109	-0.823	7.155	0.148	0.178	0.196
6.250	2.225	0.417	-0.099	-0.836	7.297	0.142	0.172	0.193
6.667	2.228	0.417	-0.097	-0.848	7.368	0.134	0.164	0.191
7.143	2.203	0.419	-0.091	-0.855	7.212	0.134	0.169	0.190
7.692	2.176	0.416	-0.072	-0.866	6.935	0.130	0.174	0.193
8.333	2.123	0.413	-0.060	-0.855	6.425	0.125	0.178	0.194
9.091	2.079	0.412	-0.049	-0.857	6.184	0.132	0.190	0.200
10.000	2.027	0.413	-0.047	-0.846	5.804	0.132	0.197	0.207

TABLE 3.9

V_{ea} 10% Damping

Regression coefficients refer to Equation 3.7, for the base 10 logarithm of motion, randomly oriented horizontal component (cm/sec)

Freq. (Hz)	a	b	c	d	h	e	f	σ
0.500	1.712	0.610	-0.048	-0.643	3.040	0.256	0.436	0.269
0.526	1.727	0.605	-0.053	-0.646	3.219	0.265	0.445	0.268
0.556	1.742	0.598	-0.057	-0.648	3.384	0.272	0.451	0.266
0.588	1.764	0.592	-0.058	-0.653	3.468	0.275	0.453	0.264
0.625	1.790	0.584	-0.053	-0.663	3.481	0.275	0.453	0.260
0.667	1.813	0.574	-0.047	-0.672	3.419	0.275	0.450	0.256
0.714	1.831	0.562	-0.048	-0.666	3.263	0.267	0.438	0.254
0.769	1.843	0.549	-0.057	-0.651	3.055	0.255	0.424	0.250
0.833	1.862	0.538	-0.064	-0.640	3.052	0.243	0.411	0.245
0.909	1.883	0.521	-0.057	-0.637	3.189	0.234	0.399	0.240
1.000	1.921	0.512	-0.052	-0.650	3.272	0.222	0.380	0.235
1.053	1.944	0.510	-0.052	-0.661	3.239	0.217	0.372	0.235
1.111	1.962	0.507	-0.052	-0.670	3.160	0.215	0.369	0.235
1.176	1.970	0.504	-0.055	-0.673	3.049	0.214	0.366	0.234
1.250	1.981	0.502	-0.058	-0.678	2.972	0.212	0.363	0.234
1.333	2.003	0.498	-0.060	-0.691	3.015	0.210	0.362	0.235
1.429	2.031	0.490	-0.062	-0.704	3.192	0.208	0.360	0.238
1.538	2.058	0.479	-0.064	-0.712	3.408	0.203	0.353	0.237
1.667	2.070	0.465	-0.067	-0.709	3.555	0.202	0.344	0.235
1.818	2.076	0.440	-0.057	-0.701	3.761	0.203	0.336	0.229
2.000	2.083	0.427	-0.055	-0.702	4.109	0.205	0.330	0.226
2.083	2.084	0.423	-0.057	-0.699	4.154	0.203	0.325	0.224
2.174	2.085	0.419	-0.060	-0.695	4.132	0.199	0.316	0.223
2.273	2.090	0.415	-0.063	-0.693	4.112	0.193	0.305	0.222
2.381	2.100	0.409	-0.064	-0.696	4.159	0.187	0.293	0.220
2.500	2.116	0.403	-0.063	-0.702	4.286	0.179	0.280	0.218
2.632	2.134	0.399	-0.065	-0.710	4.430	0.169	0.266	0.216
2.778	2.151	0.401	-0.071	-0.718	4.618	0.165	0.254	0.215
2.941	2.163	0.404	-0.079	-0.725	4.855	0.162	0.245	0.213
3.125	2.168	0.409	-0.087	-0.729	5.079	0.162	0.239	0.210
3.333	2.172	0.418	-0.097	-0.734	5.357	0.161	0.233	0.206
3.571	2.185	0.422	-0.102	-0.745	5.848	0.156	0.220	0.200
3.846	2.193	0.424	-0.102	-0.757	6.185	0.152	0.208	0.197
4.167	2.201	0.427	-0.101	-0.770	6.384	0.145	0.195	0.195
4.545	2.206	0.431	-0.105	-0.778	6.624	0.140	0.181	0.192
5.000	2.227	0.436	-0.112	-0.796	7.049	0.130	0.164	0.191
5.263	2.228	0.435	-0.114	-0.804	7.092	0.129	0.164	0.191
5.556	2.220	0.431	-0.111	-0.812	7.117	0.135	0.168	0.190
5.882	2.209	0.426	-0.106	-0.820	7.172	0.141	0.174	0.189
6.250	2.200	0.422	-0.100	-0.827	7.175	0.140	0.173	0.188
6.667	2.189	0.421	-0.095	-0.835	7.140	0.137	0.172	0.187
7.143	2.170	0.419	-0.087	-0.843	7.004	0.135	0.174	0.187
7.692	2.142	0.419	-0.075	-0.849	6.745	0.132	0.178	0.189
8.333	2.103	0.417	-0.064	-0.847	6.399	0.129	0.183	0.192
9.091	2.059	0.416	-0.054	-0.845	6.064	0.131	0.191	0.197
10.000	2.013	0.419	-0.050	-0.839	5.746	0.132	0.199	0.204

TABLE 3.10

Modal Events for the Point Source Example

	PSV				V_{ea}			
P(G>g) = 1/2,500, 60 km								
Freq.	**g**	**m'**	**m**	**ε**	**g**	**m'**	**m**	**ε**
0.5	16.7	7.46	7.08	1.12	30.6	7.46	7.03	1.20
1.0	19.0	7.30	7.03	1.24	34.1	7.46	6.97	1.28
2.0	15.8	7.03	6.70	1.68	31.8	7.30	7.03	1.24
3.0	13.8	6.70	6.54	1.80	29.8	7.03	6.86	1.40
4.0	10.8	6.59	6.50	1.80	25.5	7.03	6.86	1.40
5.0	9.9	6.49	6.43	1.80	24.8	6.97	6.81	1.44
6.7	6.6	6.38	6.27	1.96	18.5	7.03	6.92	1.32
P(G>g) = 1/500, 10 km								
Freq.	**g**	**m'**	**m**	**ε**	**g**	**m'**	**m**	**ε**
0.5	24.9	6.86	6.49	1.00	40.0	6.86	6.54	0.88
1.0	33.5	6.70	6.38	1.16	52.6	6.86	6.54	0.88
2.0	34.0	6.54	6.22	1.36	59.1	6.76	6.32	1.24
3.0	32.7	6.32	6.11	1.44	61.0	6.59	6.27	1.28
4.0	27.1	6.27	6.16	1.32	55.1	6.65	6.43	1.00
5.0	24.8	6.27	6.16	1.28	54.2	6.65	6.32	1.16
6.7	17.8	6.16	6.00	1.48	43.6	6.65	6.43	1.00

TABLE 3.11

Modal Events for the Example of Combined Background and Line Source

Background

	PSV			V_{ea}		
Freq.	**g**	**($\underline{m}'$, $\underline{r}'$)**	**($\underline{m}$, $\underline{r}$, $\underline{\varepsilon}$)**	**g**	**($\underline{m}'$, $\underline{r}'$)**	**($\underline{m}$, $\underline{r}$, $\underline{\varepsilon}$)**
0.5	24.5	(6.48, 6.5)	(6.43, 10.5, 1.08)	43.0	(6.48,6.5)	(6.48, 10.5, 1.12)
1.0	27.9	(6.43, 6.5)	(6.23, 8.5, 0.92)	47.2	(6.48, 7.5)	(6.43, 11.5, 1.00)
2.0	25.0	(5.92, 5.5)	(5.58, 5.5, 1.16)	46.1	(6.28, 6.5)	(5.93, 7.5, 1.12)
3.0	22.8	(5.73, 5.5)	(5.63, 7.5, 1.16)	44.8	(6.24, 6.5)	(5.83, 7.5, 1.08)
6.7	12.0	(5.93, 9.5)	(5.73, 10.5, 1.16)	28.8	(6.23, 8.5)	(6.03, 9.5, 0.72)

Line Source

Freq.	**g**	**($\underline{m}'$, $\underline{r}'$)**	**($\underline{m}$, $\underline{r}$, $\underline{\varepsilon}$)**	**g**	**($\underline{m}'$, $\underline{r}'$)**	**($\underline{m}$, $\underline{r}$, $\underline{\varepsilon}$)**
0.5	24.5	(7.38, 30.5)	(6.98, 30.5, 1.16)	43.0	(7.38, 30.5)	(7.08, 30.5, 0.96)
1.0	27.9	(7.28, 30.5)	(6.98, 30.5, 1.12)	47.2	(7.28, 30.5)	(6.93, 30.5, 1.16)
2.0	25.0	(6.93, 30.5)	(6.73, 30.5, 1.52)	46.1	(7.13, 30.5)	(6.93, 30.5, 1.16)
3.0	22.8	(6.48, 30.5)	(6.48, 30.5, 1.76)	44.8	(6.88, 30.5)	(6.73, 30.5, 1.40)
6.7	12.0	(6.43, 30.5)	(6.38, 30.5, 1.76)	28.8	(6.93, 30.5)	(6.78, 30.5, 1.24)

Chapter 4: Results and Conclusions

The solutions of many earthquake engineering problems involve dynamic analyses using ground-motion time series. The time series, or design earthquake, should be selected to reflect the characteristics of potential ground-motion at a specific site. Important characteristics include amplitude of motion, frequency content and duration of shaking, all of which are highly dependent upon the magnitude and distance of the earthquake. In most cases, a complete assessment of the seismic hazard must take into account the possible occurrence of earthquakes covering a range of magnitudes, and occurring at several possible distances from a given site.

The design earthquake selection problem is fundamentally probabilistic. A rational and objective apporach to the solution can involve disaggregation of a formal probabilistic model of the seismic hazard. The disaggregation can identify the most likely earthquake scenario(s), in terms of magnitude and distance, that contribute to hazard, for any specified return period. An ensemble of time series for different harmonic oscillators can be selected on the basis of the modal earthquakes derived from the analysis. This gives a useful time-domain realization of the seismic hazard, to the extent that important characteristics of the time series are correlated with the basis variable used in the analysis. A limitation may arise because most currently available motion prediction models are essentially independent of duration, and modal events based on PSHA disaggregation using peak elastic response as the basis variable for the analysis may not represent the optimal characterization of the hazard.

The elastic input energy spectrum is an attractive alternative to the elastic response spectrum for these types of analyses. The input energy combines the elements of amplitude and duration into a single parameter description of the ground motion that can be readily incorporated into standard PSHA methodology. This use of the elastic input-energy spectrum was examined, using strong motion data from Western North America. Regression modeling using consistent processing procedures for the absolute input energy equivalent velocity V_{ea}, and the elastic response PSV in the frequency range 0.5 to 10 Hz shows that the two parameters can be successfully fit with identical functional forms. The variance of V_{ea} is uniformly less than that of PSV, indicating that Vea can be predicted with slightly less uncertainty, as a function of magnitude, distance and site classification. The dependence of V_{ea} and PSV upon NEHRP site classification (BSSC, 1994) is virtually identical. The effects of site class are important at frequencies less than a few Hertz. The

regression modeling does not resolve significant effects due to site class at frequencies greater than approximately 5 Hz. These results are illustrated in Figures 3.7 through 3.9.

The elastic input energy offers a potential advantage over the elastic response spectrum in that it reflects, by integration, the effect of ground motion duration. This is evident in the regression models by a stronger magnitude scaling of V_{ea}, compared to PSV, for oscillator frequencies greater than approximately 2 Hz (Figures 3.9 through 3.11). The implication for probabilistic hazard analysis is that if the hazard is assessed on the basis of V_{ea}, the hazard posed by the larger magnitude earthquakes contributes more to the total hazard, than would be the case if the assessment where done on the basis of the elastic response spectrum. Disaggregation of simple, fairly general, seismic hazard models using V_{ea} indicates that the modal magnitudes for the higher frequency oscillators tend to be larger, and vary less with oscillator frequency, than those derived using PSV (Figures 3.12 and 3.13). Insofar as the elastic input-energy may be a better parameter for quantifying the damage potential of ground motion, its use in probabilistic seismic hazard analysis could provide an improved means for selecting earthquake scenarios and establishing design earthquakes for many types of engineering analyses.

Bibliography

Abrahamson, N. A. and K. M. Shedlock (1997). Some comparisons between recent ground-motion relations, *Seismological Research Letters*, **68**, 9-23.

Bazzurro, P. and C. A. Cornell (1998). On disaggregation of seismic hazard, submitted to *Bull. Seism. Soc. Am.*, 1998.

Bender, B. (1984). Seismic hazard estimation using a finite-fault rupture model, *Bull. Seism. Soc. Am*. **74**, 1899-1923.

Bernreuter, D. L., J. B. Savy, R. W. Mensing and J. C. Chen (1989). *Seismic Hazard Characterization of 69 Nuclear Power Plant Sites East of the Rocky Mountains.* U. S. Nuclear Regulatory Commission, NUREG/CR-5250.

Boore, D. M., W. B. Joyner, and T. E. Fumal (1997). Equations for estimating horizontal response spectra and peak acceleration from western North American earthquakes: a summary of recent work, *Seismological Research Letters*, **88**, no. 1, 128-153.

Boore, D. M., W. B. Joyner, and T. E. Fumal (1994). Estimation of response spectra and peak accelerations from western North American earthquakes: An interim report, Part 2, *U.S. Geol. Survey Open-File Report*, 94-127, 40 pp.

Boore, D. M., W. B. Joyner, and T. E. Fumal (1993). Estimation of response spectra and peak accelerations from western North American earthquakes: An interim report, *U.S. Geol. Survey Open-File Report*, 93-509, 72 pp.

BSSC (1994). NEHRP recommended provisions for seismic regulations for new buildings, Part 1 - Provisions, *FEMA 222A*, Federal Emergency Management Agency, 290 pp.

Campbell, K. W. (1997). Empirical near-source attenuation relationships for horizontal and vertical components of peak ground acceleration, peak ground velocity, and pseudo-absolute acceleration response spectra, *Seismological Research Letters*, **68**, 154-179.

Chapman, M. C. (1995) A probabilistic approach to ground-motion selection for engineering design, *Bull. Seism. Soc. Am.*, **85**, 937-942.

Cockerham, R. S., and J. P. Eaton (1987). The earthquake and its aftershocks, April 24 through September 30, 1984, in The Morgan Hill, California Earthquake of April 24, 1984, *U. S., Geological Survey Bulletin 1639*, 15-28.

Coppersmith, K. J. and R. R. Youngs (1986) Capturing uncertainty in probabilistic seismic hazard assessments within intraplate tectonic environments, *Proceedings of the Third U. S. National Conference on Earthquake Engineering*, Charleston, SC, 1, 301-312.

Cornell, C. A. (1968). Engineering seismic risk analysis, *Bull. Seism. Soc. Am.*, **58**, 1583-1606.

Cramer C. H. and M. D. Petersen (1996). Predominant seismic source distance and magnitude maps for Los Angeles, Orange and Ventura Counties, California, *Bull. Seism. Soc. Am.*, **86**, 1645-1649.

Frankel, A., C. Mueller, T. Barnhard, D. Perkins E. V. Leyendecker, N. Dickman, S. Hanson and M. Hopper (1996). National Seismic-Hazard Maps: Documentation June 1996, *U. S. Geological Survey Open-File Report 96-532*, Denver, CO.

Gutenberg, B., and C. F. Richter (1954). *Seismicity of the Earth*, Princeton University Press, 2nd ed., pp. 16-25.

Harmsen, S. C. (1997). Determination of site amplification in the Los Angeles urban area from inversion of strong-motion records, *Bull. Seism. Soc. Am.*, **87**, 866-887.

Hauksson, E., (1994). The 1991 Sierra Madre earthquake sequence in southern California: seismological and tectonic analysis, *Bull. Seism. Soc. Am.*, **84**, 1058-1074.

Joyner, W. B. and D. M. Boore (1993). Methods for regression analysis of strong-motion data, *Bull. Seism. Soc. Am.*, **83**, 469-487.

Joyner, W. B. and D. M. Boore (1994). Errata, *Bull. Seism. Soc. Am.*, **84**, 955-956.

Joyner, W. B. and D. M. Boore (1982). Prediction of earthquake response spectra, *U. S. Geol. Surv. Open File Report* 82-977.

Lawson, R. S., (1996) *Site Dependent Inelastic Seismic Demands*, Ph.D. dissertation, Department of Civil Engineering, Stanford University, Stanford, CA, 224 p.

McGuire, R. K. (1995). Probabilistic seismic hazard analysis and design earthquakes: Closing the loop, *Bull. Seism. Soc. Am.*, **85**, 1275-1284.

McGuire, R. K. and K. M. Shedlock (1981). Statistical uncertainties in seismic hazard evaluations in the United States, *Bull. Seism. Soc. Am.*, **71**, 1287-1308.

Milne, W. G. and D. H. Weichert (1986) Seismic ground-motion computations at low probabilities, *Can. J. Civ. Eng.* **13**, 595-599.

National Research Council (1988). *Proabilistic Seismic Hazard Assessment*, National Academy Press, Washington, D.C.

Nigam, N. C. and P. C. Jennings (1969). Calculation of response spectra from strong-motion earthquake records, *Bull. Seism. Soc. Am.*, **59**, 909-922.

Reiter, L. (1990). *Earthquake Hazard Analysis: Issues and Insights*, Columbia Univ. Press, New York.

Sharp, R. V., M. J. Rymer and J. J. Lienkaemper (1986). Surface displacement on the Imperial and Superstition Hill faults triggered by the Westmoreland, California earthquake of 26 April 1981, *Bull. Seism. Soc. Am.*, **76**, 949-965.

Stepp, J. C., W. J. Silva, R. K. McGuire and R. T. Sewell (1993). Determination of earthquake design loads for a high level nuclear waste repository facility, in *Proc., 4th DOE Natural Phen. Haz. Mitig. Conf.*, Vol. 2, Atlanta, GA, 651-657.

Woo, G. (1996). Kernel estimation methods for seismic hazard area source modeling, *Bull. Seism. Soc. Am.*, **86**, 353-362.

Working Group on California Earthquake Probabilities (1995). Seismic hazards in southern California: Probable earthquakes, 1994-2024, *Bull. Seism. Soc. Am.*, **85**, 379-439.

Yeats, R. S., K. Sieh and C. R. Allen (1997) *The Geology of Earthquakes*, Oxford Univ. Press, New York, 568 p.

Youngs, R. R. and K. J. Coppersmith (1985) Implications of fault slip rates and earthquake recurrence models to probabilistic seismic hazard estimates, *Bull. Seism. Soc. Am.*, **75**, 939-964.

Uang, C.-M. and V. V. Bertero (1990). Evaluation of seismic energy in structures, *Earthquake Engineering and Structural Dynamics*, **19**, 77-90.

Wald, D. J. and T. H. Heaton (1994). Spatial and temporal distribution of slip for the 1992 Landers, California, earthquake, *Bull. Seism. Soc. Am.*, **84**, 668-691.

Wald, D. J., T. H. Heaton and K. W. Hudnut (1996). The slip history of the 1994 Northridge, California, earthquake determined from strong-motion, teleseismic, GPS, and leveling data, *Bull. Seism. Soc., Am.*, **86**, no. 1B, 49-70.

Wessel, P., and W.H.F. Smith (1991). Free software helps map and display data, *EOS Trans. Amer. Geophys. U.*, **72**, 441, 445-446.

Vita

Martin C. Chapman

165 Greenway Drive
Christiansburg, VA, 24073

Education:

B.S., Geophysics, Virginia Polytechnic Institute and State University, Blacksburg VA, 1977.
M.S., Geophysics, Virginia Polytechnic Institute and State University, Blacksburg VA, 1979.
Ph.D., Geophysics, Virginia Polytechnic Institute and State University, Blacksburg VA, 1998.

Professional Experience:

Geophysicist,	Law Engineering Testing Company, Marietta GA, (1979-1984).
Research Associate	Dept. Geological Sciences, Virginia Polytechnic Institute and State University, Blacksburg, VA, (1984-Present).